

Aligning Hyperbolic Representations: an Optimal Transport-based approach

Andrés Hoyos-Idrobo
Rakuten Institute of Technology, Paris

November 8, 2021

Abstract

Hyperbolic-spaces are better suited to represent data with underlying hierarchical relationships, e.g., tree-like data. However, it is often necessary to incorporate, through alignment, different but related representations meaningfully. This aligning is an important class of machine learning problems, with applications as ontology matching and cross-lingual alignment. Optimal transport (OT)-based approaches are a natural choice to tackle the alignment problem as they aim to find a transformation of the source dataset to match a target dataset, subject to some distribution constraints. This work proposes a novel approach based on OT of embeddings on the Poincaré model of hyperbolic spaces. Our method relies on the gyrobarycenter mapping on Möbius gyrovector spaces. As a result of this formalism, we derive extensions to some existing Euclidean methods of OT-based domain adaptation to their hyperbolic counterparts. Empirically, we show that both Euclidean and hyperbolic methods have similar performances in the context of retrieval.

1 Introduction

Hyperbolic embeddings are state-of-the-art models to learn representations of data with an underlying hierarchical structure [18]. The hyperbolic space serves as a geometric prior to hierarchical structures, tree graphs, heavy-tailed distributions, e.g., scale-free, power-law [45]. A relevant tool to implement hyperbolic space algorithms is the Möbius gyrovector spaces or Gyrovector spaces [66]. Gyrovector spaces are an algebraic formalism, which leads to vector-like operations, i.e., gyrovector, in the Poincaré model of the hyperbolic space. Thanks to this formalism, we can quickly build estimators that are well-suited to perform end-to-end optimization [6]. Gyrovector spaces are essential to design the hyperbolic version of several machine learning algorithms, like Hyperbolic Neural Networks (HNN) [24], Hyperbolic Graph NN [36], Hyperbolic Graph Convolutional NN [12], learning latent feature representations [41, 46], word embeddings [62, 25], and image embeddings [29].

Modern machine learning algorithms rely on the availability to accumulate large volumes of data, often coming from various sources, e.g., acquisition devices or languages. However, these massive amounts of heterogeneous data can entangle downstream learning tasks since the data may follow different distributions. Alignment aims at building connections between two or more disparate data sets by aligning their underlying manifolds. Thus, it leverages information across datasets. This aligning is an important class of machine learning problems, with applications as ontology matching and cross-language information retrieval [3].

Nowadays, optimal transport (OT)-based similarity measures are well-suited in matching datasets tasks as they preserve the topology of the data [53]. They estimate a transformation of the source domain sample that minimizes their average displacement to the target domain sample. These methods assume the existence of an unknown function T in a pre-specified class \mathcal{T} , which characterizes the global correspondence between spaces source and target. In practice, we are interested in learning this transformation. Typically, the selection of \mathcal{T} has to be informed by the application domain. There are several studies in OT-based aligning in the context of domain adaptation in Euclidean spaces [14, 52, 59]. Recently, [3] proposed to use OT-based similarity measures and a HNN as an estimator to align hyperbolic embeddings. Nevertheless, they mention the lack of stability of this approach due to the network’s initialization procedure, which is something we tackle in this paper.

Our contributions. In this work, we propose various novel approaches to align Poincaré embeddings based on OT. In particular, we rely on the gyrobarycenter mapping (GM) on Möbius gyrovector spaces to derive extensions to some existing Euclidean methods of OT-based domain adaptation to their hyperbolic counterparts. To our knowledge, we provide a first theoretical analysis of the consistency of the hyperbolic linear layer for the regularized hyperbolic regression problem. We establish a link within the hyperbolic linear layer and wrapped Gaussian distributions. We explore GM as a strategy to increase the stability of end-to-end minimization of the current hyperbolic OT-based approach.

Notation. We denote vectors as bold lower-case, e.g. \mathbf{a} . We write matrices using bold capital letters, e.g., \mathbf{A} . Let $\|\cdot\|$ be the ℓ_2 norm of a vector. \mathbf{A}^\top is the transpose of \mathbf{A} . Letters in calligraphic, e.g. \mathcal{P} denotes sets. We denote the $(m - 1)$ -dimensional probability simplex by Δ^m . Let n be the number of data points and $[n]$ denotes $\{1, \dots, n\}$. $\mathbf{1}_n$ is a n -dimensional vector of ones (similarly for $\mathbf{0}$). Let \mathbf{I} be the identity matrix, and $\langle \mathbf{A}, \mathbf{B} \rangle_F = \text{Tr}(\mathbf{A}^\top \mathbf{B})$.

2 Background

2.1 Optimal transport

The Monge problem. For two random variables $\mathbf{x}^s \sim \alpha$ and $\mathbf{x}^t \sim \beta$ with values in \mathcal{X}^s and \mathcal{X}^t , respectively. The Monge problem seeks a transport map $T : \mathcal{X}^s \rightarrow \mathcal{X}^t$ that assigns each point \mathbf{x}^s to a single point \mathbf{x}^t , which pushes the mass of α towards that of β (i.e., $T\# \alpha = \beta$), while minimizing the transportation cost c , e.g., the squared Euclidean distance, as follows:

$$\arg \min_T \{ \mathbb{E} [c(\mathbf{x}^s, T(\mathbf{x}^s))] \mid T\# \alpha = \beta \}, \quad c : \mathcal{X}^s \times \mathcal{X}^t \rightarrow \mathbb{R}^+. \quad (1)$$

We take α and β as empirical measures: $\alpha = \sum_{i=1}^{n^s} \mathbf{a}_i \delta_{\mathbf{x}_i^s}$ and $\beta = \sum_{j=1}^{n^t} \mathbf{b}_j \delta_{\mathbf{x}_j^t}$, where $\delta_{\mathbf{x}}$ is the Dirac at position \mathbf{x} , $\mathbf{a} \in \Delta^{n^s}$ and $\mathbf{b} \in \Delta^{n^t}$ are the weights. When α is a discrete measure, a map T satisfying the constraint may not exist, e.g., when the target measure has more points than the source measure [53].

Relaxation and regularization. The Monge problem is not always relevant to studying discrete measures (i.e., histograms) like the ones presented in this paper. The idea of the Kantorovich relaxation is to use “soft” assignments defined in terms of probabilistic couplings

$\Pi(\mathbf{a}, \mathbf{b}) = \left\{ \mathbf{M} \in \mathbb{R}_+^{n^s \times n^t} \mid \mathbf{M} \mathbf{1} = \mathbf{a}, \mathbf{M}^\top \mathbf{1} = \mathbf{b} \right\}$ that solves

$$\text{OT}(\mathbf{a}, \mathbf{b}) := \arg \min_{\mathbf{M} \in \Pi(\mathbf{a}, \mathbf{b})} \langle \mathbf{M}, \mathbf{C} \rangle_{\mathbb{F}}, \quad (2)$$

where $\mathbf{C} \in \mathbb{R}^{n^s \times n^t}$ is the cost matrix related to the cost function c . The discrete optimal transport problem is a linear program that can be solved using specialized algorithms such as the network simplex or interior-point-methods. However, the current implementation of these algorithms has cubic complexity in the size of the support of α and β [48]. [16] proposed to add an entropic regularization to speed-up computations, namely

$$W_\epsilon(\mathbf{a}, \mathbf{b}) := \min_{\mathbf{M} \in \Pi(\mathbf{a}, \mathbf{b})} \langle \mathbf{M}, \mathbf{C} \rangle_{\mathbb{F}} - \epsilon H(\mathbf{M}), \quad (3)$$

where $\epsilon \geq 0$ is the regularization parameter, and $H(\mathbf{M})$ denotes the discrete entropy of a coupling matrix [53], $H(\mathbf{M}) = -\sum_{i,j} \mathbf{M}_{i,j} (\log(\mathbf{M}_{i,j}) - 1)$, with the convention: $H(a) = -\infty$ if a is 0 or negative. The Sinkhorn algorithm [16] solves Eq. 3 and can be differentiated using automatic differentiation. However, Eq. 3 is not a divergence, i.e., $W_\epsilon(\alpha, \alpha) \neq 0$. [26] proposes a divergence that overcomes the issues of the entropic regularization, the Sinkhorn divergence: $SD_\epsilon(\alpha, \beta) := W_\epsilon(\alpha, \beta) - \frac{1}{2} (W_\epsilon(\alpha, \alpha) + W_\epsilon(\beta, \beta))$.

In practice, we encode supervision by enforcing $\mathbf{C}_{i,j} = 0$ whenever \mathbf{x}_i^s matches \mathbf{x}_j^t and ∞ otherwise [14].

Barycenter mapping. Once we obtain a transport coupling \mathbf{M} using either Eq. 2 or 3, we can express the transported samples from the source as barycenters of the target samples [20, 13, 52]. This barycentric projection corresponds to solving $\hat{\mathbf{x}}_i^s = \arg \min_{\mathbf{x} \in \mathcal{X}^t} \sum_{j=1}^{n^t} \mathbf{M}_{i,j} c(\mathbf{x}, \mathbf{x}_j^t)$, which has a closed-form solution if c is the squared ℓ_2 distance, and it corresponds to a weighted average:

$$\hat{\mathbf{X}}^s = B_{\mathbf{M}}^E(\mathbf{X}^s) = \text{diag}(\mathbf{M} \mathbf{1}_{n^t})^{-1} \mathbf{M} \mathbf{X}^t. \quad (4)$$

In particular, assuming uniform sampling, it reduces to $\hat{\mathbf{X}}^s = n^s \mathbf{M} \mathbf{X}^t$. Thus, we map the source sample into the convex hull of the target examples. We use the barycenter mapping as a reference to learn an approximate transport function [52, 59].

2.2 Learning in Hyperbolic Spaces

Hyperbolic spaces. The hyperbolic space is a Riemannian manifold of constant negative curvature. A Riemannian manifold is a smooth manifold \mathcal{M} of dimension d that can be locally approximated by an Euclidean space \mathbb{R}^d . At each point $\mathbf{x} \in \mathcal{M}$ one can define a d -dimensional vector space, the tangent space $T_{\mathbf{x}}\mathcal{M}$. We characterize the structure of this manifold by a Riemannian metric, which is a collection of scalar products $\rho = \{\rho(\cdot, \cdot)_{\mathbf{x}}\}_{\mathbf{x} \in \mathcal{M}}$, where $\rho(\cdot, \cdot)_{\mathbf{x}} : T_{\mathbf{x}}\mathcal{M} \times T_{\mathbf{x}}\mathcal{M} \rightarrow \mathbb{R}$. The Riemannian manifold is a pair (\mathcal{M}, ρ) [60, 49].

The tangent space linearizes the manifold at a point $\mathbf{x} \in \mathcal{M}$, making it suitable for practical applications as it leverages the implementation of algorithms in the Euclidean space. We use the Riemannian exponential and logarithmic maps to project samples onto the manifold and back to tangent space, respectively. The Riemannian exponential map, when well-defined, $\text{Exp}_{\mathbf{x}} : T_{\mathbf{x}}\mathcal{M} \rightarrow \mathcal{M}$ realizes a local diffeomorphism from a sufficiently small neighborhood $\mathbf{0}$ in $T_{\mathbf{x}}\mathcal{M}$ into a neighborhood of the point $\mathbf{x} \in \mathcal{M}$. The logarithmic map is the inverse exponential map, $\text{Log}_{\mathbf{x}} : \mathcal{M} \rightarrow T_{\mathbf{x}}\mathcal{M}$.

There are five isometric models of the hyperbolic manifold [10]. Our focus is on the Poincaré ball model because of the Möbius gyrovector formalism (see below). The Poincaré

ball $\mathbb{B}_s^d = \{\mathbf{x} \in \mathbb{R}^d : \|\mathbf{x}\|^2 < s, s \geq 0\}$ has the Riemannian metric $\rho_{\mathbf{x}^s}^{\mathbb{B}_s} = (\lambda_{\mathbf{x}}^s)^2 \rho^E$, where $\lambda_{\mathbf{x}}^s := 2 / (1 - \|\mathbf{x}\|^2 / s)$, and $\rho^E = \mathbf{I}_d$ is the Euclidean metric tensor. Hence, the conformal factor $\lambda_{\mathbf{x}}^s$ [49] connects the Euclidean space and the Poincaré ball.

Gyrovector formalism. Gyrovector spaces analogize Euclidean vector spaces and provide a non-associative algebraic formalism for the hyperbolic geometry of the Poincaré model [66, 24]. Let $(\mathbb{B}_s^d, \oplus_s, \otimes_s)$ be a Möbius gyrovector space with Möbius addition \oplus_s and Möbius product \otimes_s . These operations and their properties are described in closed-forms in Section 4 in supp. mat. A remark, the Möbius addition \oplus_s is often non-commutative, $-(\mathbf{u} \oplus_s \mathbf{v}) \oplus_s \mathbf{u} \neq \mathbf{v}$. However, we can subtract using this operation from the left, $-\mathbf{u} \oplus_s (\mathbf{u} \oplus_s \mathbf{v}) = \mathbf{v}$. This is known as the left-cancellation law [66].

The Poincaré distance $d_s : \mathbb{B}_s^d \times \mathbb{B}_s^d \rightarrow \mathbb{R}_+$ [67] is:

$$d_s(\mathbf{x}, \mathbf{y}) = 2s \tanh^{-1} \left(\frac{\|\mathbf{x} \oplus_s \mathbf{y}\|}{s} \right). \quad (5)$$

We use wrap functions to compute functions on the manifold [24]. Let $f : \mathbb{R}^d \rightarrow \mathbb{R}^p$ then the Möbius version of f that maps from \mathbb{B}^d to \mathbb{B}^m is defined by:

$$f^{\otimes_s}(\mathbf{x}) = \text{Exp}_{\mathbf{0}}(f(\text{Log}_{\mathbf{0}}(\mathbf{x}))). \quad (6)$$

We obtain the Möbius matrix-vector multiplication by using a linear map $\mathbf{Q} : \mathbb{R}^d \rightarrow \mathbb{R}^p$ in Eq. 6, $\mathbf{Q}^{\otimes_s} \mathbf{x}$.

Hyperbolic neural networks (HNN). As their Euclidean counterpart, hyperbolic neural networks [24] rely on a sequence of matrix-vector multiplications followed by an element-wise non-linearity. For $i > 0$ hidden layers,

$$\mathbf{h}^{(i)} = \sigma_{\mathbb{B}} \left(\underbrace{\mathbf{b}^{(i)} \oplus_s \left(\left(\mathbf{W}^{(i)} \right)^{\otimes_s} \mathbf{h}^{(i-1)} \right)}_{\text{Hyperbolic linear layer}} \right), \quad (7)$$

where $\mathbf{W}^{(i)} \in \mathbb{R}^{d^{(i)} \times d^{(i-1)}}$ is the weight matrix, $\mathbf{b}^{(i)} \in \mathbb{B}_s^{d^{(i)}}$ the bias term, and $\sigma_{\mathbb{B}}(\cdot)$ is a Möbius function in the form of Eq. 6 with a standard non-linearity, e.g., ReLU. The intermediate layers of the network do not need to have the same dimension. Here, we use the left Möbius addition instead of the right one [24]. As for our analysis, we rely heavily on the left cancellation-rule (See Section 5 in supp. mat.).

Gyrobarycenter mapping (GM). The gyrobarycentric coordinates are the hyperbolic version of the Euclidean barycentric coordinates. The hyperbolic graph neural networks [28, 29, 4] use GM in the aggregation step. We propose a matrix version of the gyrobarycentric coordinates in Möbius Gyrovector Spaces [1],

$$B_M^H(\mathbf{X}^s) = \frac{1}{2} \otimes_s \text{diag}(\mathbf{M} \mathbf{g})^{-1} \mathbf{M} \mathbf{G} \mathbf{X}^t, \quad (8)$$

where $\mathbf{g} = (\gamma_{\mathbf{X}^t}^s)^2 - \frac{1}{2}$, $\mathbf{G} = \text{diag}((\gamma_{\mathbf{X}^t}^s)^2)$, and $\gamma_{\mathbf{X}^t}^s$ denotes the Lorentz gamma factor applied sample-wise. We observe that $\lim_{s \rightarrow \infty} B_M^H(\mathbf{X}^s) = \frac{4}{7} B_M^E(\mathbf{X}^s)$, i.e., we recover Euclidean barycenter in the limit¹.

¹The factor $\frac{7}{4}$ comes from the distortion induced by the conformal factor $\gamma_{\mathbf{x}}^s$. See Section 5 in supp. mat.

GM is a geodesically-convex combination of target samples. Empirically, the gyromidpoint (i.e., gyrobarycenter with uniform weights) is close to the Fréchet/Karcher mean [11]. The Fréchet mean is the point with minimum weighted mean squared-Riemannian distance to all the set [23]. Contrary to the gyrobarycenter, it has no closed-solution. We rely on iterative algorithms to compute the Fréchet mean [50], which can be prohibitively expensive, especially when one requires gradients to flow through the solution.

Hyperbolic OT. We introduced OT problems in Section 2.1, which defines the minimum cost assignment between two Euclidean spaces. Then, the question is whether or not OT extends to hyperbolic spaces. The answer is partially positive [3, 43]. In hyperbolic spaces, there is no guarantee for the smoothness of the transport map for the usual cost $d_s(\mathbf{x}, \mathbf{y})^2$ for $\mathbf{x}, \mathbf{y} \in \mathbb{B}_s^d$. However, we use compositions of a function l with the Riemannian distance, e.g., $-\cosh \circ d$ [35, 34]. We provide more details in Section 3 of supp. mat. Fig. 1 shows an illustration of the Euclidean and hyperbolic OT.

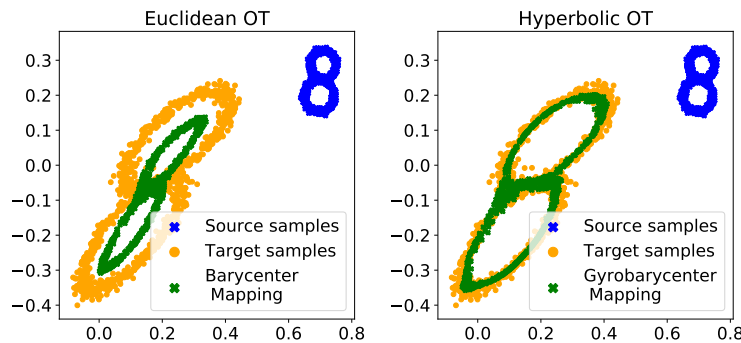


Figure 1: **Illustration:** We obtain the probabilistic coupling using Euclidean OT-problem (*left*) and Hyperbolic OT-problem (*right*). We set $\epsilon = 0.01$ for both methods.

3 Related work

Mapping estimation (ME). These methods avoid direct minimization of OT-based similarity measures, like Eq. 3 or the Sinkhorn divergence. Instead, they alternate between approximating the barycenter projection and the transport plan. ME uses different and often problem-dependent estimators for the approximation. Some estimators in the literature are Nearest neighbors (OT domain adaptation, OT-DA)[14], Kernel methods [52], and Neural Networks [59]. A particular case is the linear mapping, which has closed-solution [53, 22]. As far as we know, there is no adaptation/implementation of these approaches in hyperbolic spaces, which is part of our contribution.

Direct minimization of OT-loss (OT-Direct). These methods minimize the OT-based similarity measure between target samples and transformed source samples. This idea is present in the Euclidean case in several OT-based algorithms for domain adaptation [15, 17]. More recently, [3] proposes an unsupervised approach to match points in two different Poincaré spaces. [3] optimizes the OT-loss and the transport map simultaneously, using as a loss either $W_\epsilon(\alpha, T_{\frac{1}{2}}(\beta))$ or $SD_\epsilon(\alpha, T_{\frac{1}{2}}(\beta))$ with a suitable hyperbolic cost, where T is a HNN. However, this approach is sensitive to initialization due to both the objective function

and HNN’s nature [25]. They propose three pre-training initialization to increase robustness to initialization:

- **Permutation.** The map approximately matches a random permutation of target samples:

$$T \leftarrow \arg \min_T \frac{1}{n^s} \sum_{i=1}^{n^s} d_s(\mathbf{x}_{\sigma(i)}^t, T(\mathbf{x}_i^s)), \quad (9)$$

for some permutation $\sigma(i)$.

- **Identity.** The map approximately preserves the geometry of the source space:

$$T \leftarrow \arg \min_T \frac{1}{n^s} \sum_{i=1}^{n^s} d_s(\mathbf{x}_i^s, T(\mathbf{x}_i^s)). \quad (10)$$

- **Procrustes.** The map is approximately a rotation of the source space:

$$T \leftarrow \arg \min_T \frac{1}{n^s} \sum_{i=1}^{n^s} d_s(\mathbf{P} \mathbf{x}_i^s, T(\mathbf{x}_i^s)), \quad (11)$$

where $\mathbf{P} = \arg \min_{\mathbf{P}^\top \mathbf{P} = \mathbf{I}} \|\mathbf{X}^t - \mathbf{P} \mathbf{X}^s\|_{\mathbb{F}}^2$.

Here, we introduce the GM as initialization strategy to reduce the lack of stability due to initialization:

$$T \leftarrow \arg \min_T l^H(T, B_{\mathbf{M}}^H) := \frac{1}{n^s} \sum_{i=1}^{n^s} d_s(B_{\mathbf{M}}^H(\mathbf{x}_i^s), T(\mathbf{x}_i^s)), \quad (12)$$

where $l^H(T, B_{\mathbf{M}}^H)$ is the fitting data term, which assess the quality of the map to reconstruct a given GM. Our motivation follows Procrustes initialization. Instead of finding a rotation, we use the GM which, represents a possibly highly nonlinear approximation encoded in the probabilistic coupling \mathbf{M} . The GM initialization requires solving Eq. 2 or 3, making it significantly more computationally expensive than the other three pre-training approaches.

4 Aligning Hyperbolic Representations

4.1 Hyperbolic OT-DA

We also extend the Euclidean OT-DA algorithm [14, 20] to its hyperbolic version. The most straightforward OT-DA algorithm uses a nearest-neighbor interpolation approach. While training, this algorithm memorizes the barycenter mapping of a given set of source samples. If a new sample does not belong to the training set, the algorithm uses the nearest-neighbor interpolation of the barycenter mapping. In our extension, we replace the barycenter by the GM and rely on a Möbius-based nearest-neighbor interpolation. Hence, $T(\mathbf{x}) = B_{\mathbf{M}}^H(\mathbf{X}_{i(\mathbf{x})}^s) \oplus_s (-\mathbf{X}_{i(\mathbf{x})}^s \oplus_s \mathbf{x})$ where $i(\mathbf{x}) = \arg \min_{i \in [n^s]} d_s(\mathbf{x}, \mathbf{X}_i^s)$.

4.2 Hyperbolic Mapping Estimation

Our hyperbolic mapping estimation (Hyp-ME) definition is inspired by and extends the Euclidean mapping estimation framework [52, 59] to the hyperbolic setting. Hyp-ME aims at finding a transport map between two hyperbolic representations using the GM as a proxy. We use a loss composed of two global terms: a fitting data term for the transport map and an OT-loss for the GM, each with its regularization term. Thus, the total loss of the Hyp-ME is:

$$g(\mathbf{M}, T) := \underbrace{\left(l^{\text{H}}(T, B_{\mathbf{M}}^{\text{H}}) + \omega \Omega(T) \right)}_{\text{Quality of the mapping}} + \eta \underbrace{\left(\langle \mathbf{M}, \mathbf{C} \rangle_{\text{F}} - \epsilon H(\mathbf{M}) \right)}_{\text{Regularized OT}}, \quad (13)$$

where $\Omega(\cdot)$ is a regularization term and $\eta \geq 0$, $\omega \geq 0$ are hyper-parameters. In particular, η controls the trade-off between the two groups of terms in the loss. We obtain T and \mathbf{M} by solving the following optimization problem

$$(\mathbf{M}, T) \leftarrow \arg \min_{T \in \mathcal{T}, \mathbf{M} \in \Pi(\mathbf{a}, \mathbf{b})} g(\mathbf{M}, T), \quad (14)$$

where \mathcal{T} is the space of transformations from \mathcal{X}^{s} to \mathcal{X}^{t} .

Optimization procedure. We rely on alternate optimization w.r.t. both parameters \mathbf{M} and T . This algorithm well-known as Block Coordinate Descent [64]. Algorithm 1 shows the steps of our optimization procedure. We note that the GM couples both groups of terms. Thus, minimizing the total loss with a fixed transport map boils down to a constrained OT-problem (see Eq. 15). We rely on a generalized conditional gradient descent algorithm (GCG) [14, 54, 9]. We repeat alternating until we satisfy some convergence criterion. We are not insured to converge to the optimal solution as the data fit term is only convex when $s \rightarrow \infty$. However, the algorithm works well in practice.

Algorithm 1 Hyp-ME with Block Coordinate Descent

Require: Initial transport map \hat{T} , cost matrix \mathbf{C}

Ensure: Stationary point of Eq. 14

1: **while** not converge **do**

2: **Update M:** with a fixed estimator \hat{T} ,

$$\hat{\mathbf{M}} \leftarrow \arg \min_{\mathbf{M} \in \Pi(\mathbf{a}, \mathbf{b})} \eta (\langle \mathbf{M}, \mathbf{C} \rangle_{\text{F}} - \epsilon H(\mathbf{M})) + l^{\text{H}}(\hat{T}, B_{\mathbf{M}}^{\text{H}}). \quad (15)$$

3: **Update T:** with a fixed coupling $\hat{\mathbf{M}}$,

$$\hat{T} \leftarrow \arg \min_{T \in \mathcal{T}} l^{\text{H}}(T, B_{\hat{\mathbf{M}}}^{\text{H}}) + \omega \Omega(T). \quad (16)$$

4: **end while**

Updating M. In our case, the GCG algorithm uses a partial linearization of the Hyp-ME loss (Eq. 13) w.r.t. \mathbf{M} to build a sequence of linear minimization problems. Thus, for each iteration k , we compute the following linear oracle:

$$\mathbf{M}^* \leftarrow \arg \min_{\mathbf{M} \in \Pi(\mathbf{a}, \mathbf{b})} \langle \mathbf{M}, \mathbf{F}^k \rangle_{\text{F}} - \hat{\epsilon} H(\mathbf{M}), \quad (17)$$

where $\mathbf{F}^k = \eta \mathbf{C} + (\lambda_{\text{GM}}^s)^{-2} \nabla_{\mathbf{M}} l^{\text{H}}(\hat{T}, B_{\mathbf{M}}^{\text{H}}) \Big|_{\mathbf{M}=\mathbf{M}^k}$, $\hat{\epsilon} = \eta \epsilon$, and λ_{GM}^s is the conformal factor at the point mapped by the GM. This factor links the hyperbolic and the Euclidean gradient (see Section 2.2). Eq. 17 is a regularized OT-problem with a modified cost function. We update the map by computing $\mathbf{M}^{k+1} = \mathbf{M}^k + \alpha^k (\mathbf{M}^* - \mathbf{M}^k)$, where α^k is the optimal step that satisfies the Armijo rule that minimizes Eq. 13. We repeat until reaching some local convergence criterion.

Updating T . The Hyp-ME considers a broad set of transformations \mathcal{T} . We use HNN. Thus, we rely on algorithms based on Riemannian gradient descent [6] to minimize Eq. 16, which is possible given that we have access to closed-form implementations of the gyrovector and Riemannian-based operations (see Section 2.2).

4.3 Analysis: Hyperbolic Linear Layer

In this section, we propose a novel analysis of the set of hyperbolic linear transformations induced by a real matrix $\mathbf{L} \in \mathbb{R}^{\text{d}^t \times \text{d}^s}$:

$$\mathcal{T} = \left\{ T : \exists \mathbf{L} \in \mathbb{R}^{\text{d}^t \times \text{d}^s}, \forall \mathbf{x}^s \in \mathcal{X}^s, T(\mathbf{x}^s) = (\mathbf{L}^{\otimes_s} \mathbf{x}^s)^\top \right\}. \quad (18)$$

Furthermore, we define $\Omega(T) = \|\mathbf{L} - \mathbf{K}\|_{\mathbb{F}}^2$, where \mathbf{K} is a predefined constant matrix, e.g., \mathbf{I} , which ensures that the examples are not moved far away from their initial position.

Consistency. Showing the consistency boils down to bound with high probability the true risk $R(\mathbf{L})$ by the empirical risk $\hat{R}_{\text{emp}}(\mathbf{L})$, both defined as

$$R(\mathbf{L}) = \mathbb{E}_{(\mathbf{x}, \mathbf{y})} d_s((\mathbf{L}^{\otimes_s} \mathbf{x})^\top, \mathbf{y}) \quad \text{and} \quad \hat{R}_{\text{emp}}(\mathbf{L}) = \frac{1}{n} \sum_{j=1}^n d_s((\mathbf{L}^{\otimes_s} \mathbf{x}_j)^\top, \mathbf{y}_j).$$

Note that the hyperbolic distance or its square is not geodesically convex w.r.t. Möbius matrix multiplication (see Lemma 9 in supp. mat.).

Theorem 1. *Let $\|\mathbf{y}\| \leq C_y$ and $\|\mathbf{x}\| \leq C_x$, for any \mathbf{x} and \mathbf{y} in $\mathbb{B}_s^d \setminus \{\mathbf{0}\}$ with a probability of $1 - \delta$ for any matrix \mathbf{L} optimal solution of problem 14 such that $\|\mathbf{L}\mathbf{x}\|^{-1} \leq L$ and $\|\mathbf{L}\mathbf{y}\|^{-1} \leq L$, we have:*

$$\begin{aligned} R(\mathbf{L}) \leq & \hat{R}_{\text{emp}}(\mathbf{L}) + \frac{1}{\omega n} \left(\frac{N_x^2}{4\omega n} + 2N_x + 8K_y + 1 \right) \\ & + \left(\frac{2}{\omega} \left(\frac{N_x^2}{4\omega n} + 2N_x + 1 \right) + K_y \left(\frac{K_x + 16}{\omega} + 1 \right) \right) \sqrt{\frac{\ln(1/\delta)}{2n}}, \end{aligned} \quad (19)$$

where $N_x = \sqrt{8\pi s^3 L C_x}$, $K_x = d_s(\mathbf{0}, C_x)$, and $K_y = d_s(\mathbf{0}, C_y)$.

Proof. We present the proof in supp. mat. □

Our theorem shows that the hyperbolic linear layer has a sample complexity of $O(n^{-1/2})$, the same as the Euclidean version [52, 51]. However, $s \rightarrow \infty$ does not link the bounds on the Euclidean and hyperbolic settings.

Quality of the approximation. We discuss the quality of the transport map approximation for the hyperbolic layer neural network. Similarly to [52], we have the following theorem.

Theorem 2. *Let T^* be the true transport map. Let $B_{\mathbf{M}_0}^H$ be the true GM associated with the probabilistic coupling \mathbf{M}_0 . Let $B_{\hat{\mathbf{M}}}^H$ be the empirical GM of \mathbf{X}^s using the probabilistic coupling $\hat{\mathbf{M}}$ learned between \mathbf{X}^s and \mathbf{X}^t . Then, quality of the transport map approximation is bounded as follows*

$$\begin{aligned} \mathbb{E}_{\mathbf{x}^s \sim \mathcal{X}^s} [d_s(T(\mathbf{x}^s), T^*(\mathbf{x}^s))] &\leq \sum_{\mathbf{x}^s \in \mathcal{X}^s} d_s(T(\mathbf{x}^s), B_{\hat{\mathbf{M}}}^H(\mathbf{x}^s)) \\ &+ \sum_{\mathbf{x}^s \in \mathcal{X}^s} d_s(B_{\hat{\mathbf{M}}}^H(\mathbf{x}^s), B_{\mathbf{M}_0}^H(\mathbf{x}^s)) \\ &+ \mathbb{E}_{\mathbf{x}^s \sim \mathcal{X}^s} [d_s(T^*(\mathbf{x}^s), B_{\mathbf{M}_0}^H(\mathbf{x}^s))] + O\left(\frac{1}{\sqrt{n}}\right). \end{aligned} \quad (20)$$

Proof. We present the proof in supp. mat. \square

The inequality in Eq. 20 assesses the quality of the learned transformation T w.r.t three principal quantities. We minimize the first quantity in Eq. 14. We foresee the first term to be small for families of functions with high representation power, e.g., deep HNN; however, we need to explore these families' consistency. The remaining terms are theoretical quantities that are hard to bound due to GM's lack of theory in the statistical learning context. However, we expect the second term to decrease uniformly w.r.t. the number of samples as it measures the empirical GM's quality. Assuming that the empirical GM is a good approximation, we also expect the last term to be small. We believe understanding gyrobarcenters opens up new theoretical perspectives about OT in machine learning on hyperbolic manifolds, but these are beyond the scope of this paper.

Link with wrapped Gaussians. This section shows the link between the hyperbolic linear layer and wrapped Gaussian distributions in the hyperbolic space. We start by defining wrapped Gaussian distributions. Then, we state a theorem that links both models explicitly.

Definition 1 (Wrapped Gaussian [44, 39, 58]). *Define $\mathbf{x} \sim (\text{Exp}_\mu)_\# \mathcal{N}(0, \Sigma)$ to be a wrapped Gaussian random variable with bias $\mu \in \mathbb{B}_s^d$ and covariance matrix $\Sigma \in \mathbb{R}^{n \times n}$. To build a wrapped Gaussian, we draw samples at random from a zero-mean Gaussian distribution with covariance Σ , $\mathbf{z} \sim \mathcal{N}(0, \Sigma)$. We project these samples onto the manifold at zero, $\bar{\mathbf{x}}_i = \text{Exp}_0(\mathbf{z}_i)$. Finally, we add the bias term μ using the Möbius addition, $\mathbf{x}_i = \text{Exp}_\mu(\bar{\mathbf{x}}_i)$.*

Theorem 3. *Let $\mathbf{x} \sim (\text{Exp}_{\mu_1})_\# \mathcal{N}(0, \Sigma_1)$ and $\mathbf{y} \sim (\text{Exp}_{\mu_2})_\# \mathcal{N}(0, \Sigma_2)$ be two hyperbolic random variables, distributed under wrapped Gaussian with parameters $\mu_i \in \mathbb{B}_s^d$ for $i \in [2]$ and $\Sigma_i \in \mathbb{R}^{n \times n}$ for $i \in [2]$. Then,*

$$\begin{bmatrix} \mathbf{x} \\ \mathbf{y} \end{bmatrix} \sim (\text{Exp}_{[\mu_1, \mu_2]})_\# \mathcal{N}\left(\mathbf{0}, \begin{bmatrix} \Sigma_1 & \mathbf{T} \Sigma_1 \\ \Sigma_1 \mathbf{T} & \Sigma_2 \end{bmatrix}\right), \quad (21)$$

where $\mathbf{T} = \Sigma_1^{-\frac{1}{2}} \left(\Sigma_1^{\frac{1}{2}} \Sigma_2 \Sigma_1^{\frac{1}{2}} \right)^{\frac{1}{2}} \Sigma_1^{-\frac{1}{2}}$ [7, 22]. Then, the transport map is $T(\mathbf{x}) = \mathbf{y} = \mu_2 \oplus_s \mathbf{T}^{\otimes_s}(-\mu_1 \oplus_s \mathbf{x})$.

Proof. We present the proof in supp. mat. \square

Observe that $\lim_{s \rightarrow \infty} T(\mathbf{x}) = \mu_2 + \mathbf{T}(\mathbf{x} - \mu_1)$, which is the transport map between two Gaussians [32, 53].

The main implication of Theorem 3 is that by definition (see Eq.7), a hyperbolic linear layer represents a linear Monge mapping between wrapped Gaussian distributions.

The Wrapped Linear Map (W-linear map). It is the closed-form solution given by the Theorem 3. First, we center the data by subtracting (i.e., left Möbius subtraction) the gyromidpoint of source and target, respectively. Then, we compute the Gaussian transport plan [7, 40] of the covariance matrices in the tangent space at zero, \mathbf{T} . Fig. 2 shows an illustration of the wrapped linear transport.

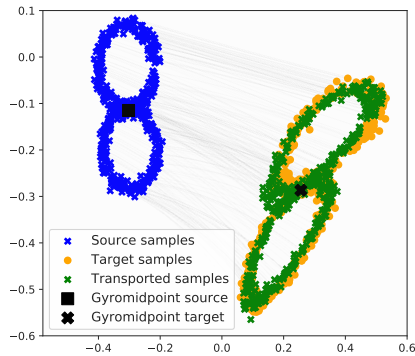


Figure 2: **Hyperbolic mapping estimation on a toy example.** Example of wrapped linear mapping estimation between empirical distributions. Lines denote the geodesics (gyrolines) of the transported samples.

5 Experiments

5.1 Setup.

Datasets. We consider two subtasks of the OAEI 2018 ontology matching challenge [2]: *Anatomy*, with two ontologies; *Biodiv*, with four². We use the *English-French*-matching task from the DBPL15k dataset [61], used for cross-lingual entity alignment (see Section 1 in the supp. mat.). For each collection, we generate embeddings in the Poincaré Ball of dimension 10 [45]. We perform a 10-fold cross-validation loop. We consider a supervised aligning task, where we train with 10% of the matched data and validate on the remaining 90%.

Baselines and metrics. We compare several OT-based alignment methods against their proposed hyperbolic counterpart: Linear mapping estimation [32], mapping estimation (ME) [52], OT-DA [14], hyperbolic OT-direct [3], Euclidean OT-direct, hyperbolic linear layer (W-linear map), and hyperbolic OT-DA, and Hyp-ME. All models return transported embeddings. Using these, we retrieve nearest neighbors under the hyperbolic distance. We report the Hits@10, which measures the percentage of times the right matched point appears in the top 10 ranked evaluation. Additionally, we report the computation time.

We use neural networks and HNN for the Euclidean and hyperbolic cases, respectively. We set 6 hidden layers, 100 hidden units with ReLU as the activation function. We initialize the weights as in [27]. We use Riemannian ADAM [6] for hyperbolic models, and ADAM [31] for the Euclidean

²oaei.ontologymatching.org/2018/

ones. In all experiment, we set the number of iterations of the Sinkhorn algorithm to be less than 100. We set the regularization parameter $\epsilon = 0.01$, and $\mathbf{a} = \mathbf{b} = \mathbf{1}_n/n$. For iterative methods, we set the stopping criteria to a relative tolerance of 1×10^{-7} .

Technical aspects. We used Gensim [57] to compute the Poincaré embeddings. We used the POT library [21] for OT related algorithms. We used the Autodiff implementation of the Sinkhorn algorithm³ for the end-to-end learning task. We relied on the geoopt package for Riemannian optimization [33]. Our methods are implemented in Pytorch [47] and are available⁴. We run all the experiments on a single desktop machine with a 4-core Intel Core i7 @2.4 GHz.

5.2 Results

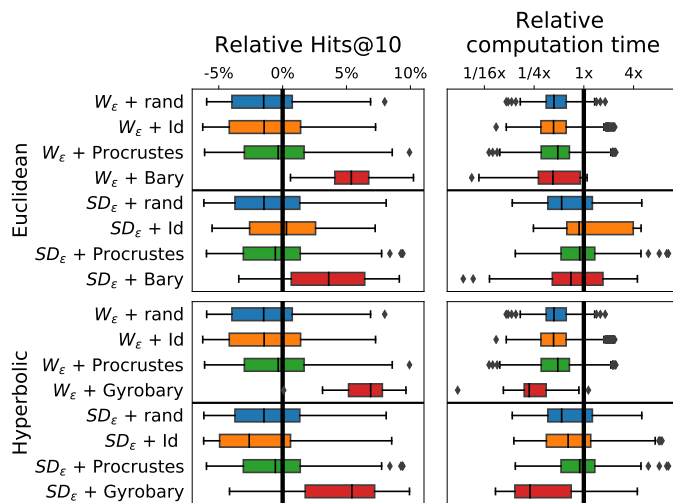


Figure 3: **Effect of various initialization in OT-direct:** Comparing different initialization approaches for Euclidean and hyperbolic estimators, using the Sinkhorn loss and Sinkhorn divergence.

Effect of the initialization in OT-direct. We explore the impact of several initialization strategies in the robustness of OT-direct: random initialization, identity mapping (Eq. 10), Procrustes alignment (Eq. 11), and barycenter/gyrobarycenter mapping (Eq. 12). We use W_ϵ and SD_ϵ as OT-based losses. The GM initialization corresponds to one step of the Algorithm 1 without taking the fitting data term ($\eta \rightarrow \infty$).

Fig. 3 displays the performance across datasets relative to the mean of both Euclidean and hyperbolic neural networks with different initialization methods with two OT-direct losses: W_ϵ and SD_ϵ . The barycenter and gyrobarycenter initialization display the best performance for all losses consistently. The random and the identity strategy exhibit similar performance in Euclidean and hyperbolic methods for all losses. The gyrobarycenter with the Sinkhorn loss has the best performance with less variance. Regarding the computation time, the gyrobarycenter is approximately two times faster than other initialization procedures. In Euclidean spaces, the barycenter method improves retrieval performance without increasing computation time. Therefore, the barycenter mapping/GM initialization provides a good proxy for the transport map. Hence, closer to the optimal value.

³github.com/gpeyre/SinkhornAutoDiff

⁴Link to the Github repository

	En-Fr			Human-Mouse			Flopo-Pto			Envo-Sweet		
	T(m)	Hits@10		T(m)	Hits@10		T(m)	Hits@10		T(m)	Hits@10	
		→	←		→	←		→	←		→	←
<i>Euclidean Methods</i>												
Linear ma [32]	< 0.1	0.47	0.47	< 0.1	0.59	0.67	< 0.1	8.77	6.81	< 0.1	2.85	2.77
OT-DA [13]	< 0.1	14.93	14.94	< 0.1	13.15	12.26	< 0.1	7.03	6.96	< 0.1	13.96	14.38
ME [52]	1.79	14.86	14.88	1.09	12.46	9.42	0.13	6.88	6.96	0.39	14.07	14.16
<i>OT-Direct</i>												
W_ϵ + Bary	0.71	3.61	3.50	3.95	11.18	8.25	0.82	6.81	6.16	1.03	13.77	12.88
SD_ϵ + Bary	0.94	3.48	3.50	11.38	11.59	7.96	1.50	6.52	6.34	2.91	13.93	13.21
<i>Hyperbolic Methods</i>												
W-linear map	< 0.1	0.36	0.36	< 0.1	0.59	0.76	< 0.1	6.88	6.96	< 0.1	2.52	2.60
OT-DA	< 0.1	14.94	14.93	< 0.1	12.97	12.80	< 0.1	6.96	6.96	< 0.1	14.52	14.93
ME	25.59	16.17	15.87	37.15	13.03	11.47	2.39	7.25	6.67	9.92	14.57	13.99
<i>OT-Direct [3]</i>												
W_ϵ + Gyrobary	5.39	3.87	3.92	1.15	12.64	9.92	0.54	6.01	6.38	1.60	14.32	13.99
SD_ϵ + Gyrobary	6.18	3.91	3.91	3.80	13.04	10.34	0.56	7.10	6.59	2.72	14.56	13.63

Table 1: Prediction on DBP15K, Anatomy, and Biodiv datasets. Color-code: the darker the better.

Retrieval. Table 1 presents the predictive performance for the supervised alignment task. The hyperbolic version of OT-DA and ME display the best performance across datasets. Their Euclidean version follows them with similar performance. In the Flopo-Pto subtask of the Biodiv dataset, the Poincaré embeddings exhibit a Gaussian-like form, explaining linear mappings’ good performance. We do not observe this in other datasets. OT-direct approaches behave poorly in the DBP15K dataset. The input vectors lie inside the unit ball; thus, the Euclidean barycenter will always be in this ball. Additionally, we use estimators with a high representation power. Therefore, we attribute the slight difference in performance between the hyperbolic and Euclidean schemes to the quality of the probabilistic coupling \mathbf{M} on each manifold.

6 Discussion

In this paper, we show that the hyperbolic layer has a sample complexity of $O(n^{-1/2})$ (Theorem 1). We then bridge the gap between the hyperbolic layer and wrapped Gaussian distributions using Theorem 3. Additionally, we proposed a closed-form solution for the transport between wrapped Gaussian distributions: the wrapped linear model. We extend to the hyperbolic space some OT-based methods for feature alignment by using gyrobarycenter mappings: Hyp-OT-DA and Hyp-ME.

In all experiments, the hyperbolic methods benefit the retrieval performance compared to the Euclidean geometry. The barycenter and gyrobarycenter initialization approaches help to avoid the estimator’s collapse while minimizing OT-based similarities directly. The wrapped linear model can align the latent space of hyperbolic wrapped variational autoencoders [41]. The analysis presented in this paper opens the door to several perspectives on machine learning on hyperbolic spaces, such as the quality and the consistency of the gyrobarycenter approximation in OT problems in hyperbolic spaces.

References

- [1] U. A. Albert. *Barycentric calculus in Euclidean and hyperbolic geometry: A comparative introduction*. World Scientific, 2010.
- [2] A. Algergawy, M. Cheatham, D. Faria, A. Ferrara, I. Fundulaki, I. Harrow, S. Hertling, E. Jiménez-Ruiz, N. Karam, A. Khiat, et al. Results of the ontology alignment evaluation initiative 2018. 2018.

- [3] D. Alvarez-Melis, Y. Mroueh, and T. S. Jaakkola. Unsupervised hierarchy matching with optimal transport over hyperbolic spaces. In *AISTATS*, 2020.
- [4] G. Bachmann, G. Bécigneul, and O.-E. Ganea. Constant curvature graph convolutional networks. In *ICML*, 2020.
- [5] A. F. Beardon, D. Minda, et al. The hyperbolic metric and geometric function theory. *Quasiconformal mappings and their applications*, 956, 2007.
- [6] G. Bécigneul and O.-E. Ganea. Riemannian adaptive optimization methods. In *ICLR*, 2019.
- [7] R. Bhatia, T. Jain, and Y. Lim. On the bures–wasserstein distance between positive definite matrices. *Expositiones Mathematicae*, 37:165–191, 2019.
- [8] O. Bousquet and A. Elisseeff. Stability and generalization. *Journal of machine learning research*, 2:499–526, 2002.
- [9] K. Bredies, D. A. Lorenz, and P. Maass. Equivalence of a generalized conditional gradient method and the method of surrogate functionals. In *University of Bremen*. Citeseer, 2005.
- [10] J. W. Cannon, W. J. Floyd, R. Kenyon, W. R. Parry, et al. Hyperbolic geometry. *Flavors of geometry*, 31:59–115, 1997.
- [11] B. P. Chamberlain, S. R. Hardwick, D. R. Wardrope, F. Dzogang, F. Daolio, and S. Vargas. Scalable hyperbolic recommender systems. *arXiv preprint arXiv:1902.08648*, 2019.
- [12] I. Chami, Z. Ying, C. Ré, and J. Leskovec. Hyperbolic graph convolutional neural networks. In *NeurIPS*, pages 4869–4880, 2019.
- [13] N. Courty, R. Flamary, and D. Tuia. Domain adaptation with regularized optimal transport. In *Joint European Conference on Machine Learning and Knowledge Discovery in Databases*, pages 274–289. Springer, 2014.
- [14] N. Courty, R. Flamary, D. Tuia, and A. Rakotomamonjy. Optimal transport for domain adaptation. *IEEE TPAMI*, 39:1853–1865, 2016.
- [15] N. Courty, R. Flamary, A. Habrard, and A. Rakotomamonjy. Joint distribution optimal transportation for domain adaptation. In *NeurIPS*, pages 3730–3739, 2017.
- [16] M. Cuturi. Sinkhorn distances: Lightspeed computation of optimal transport. In *NeurIPS*, pages 2292–2300, 2013.
- [17] B. B. Damodaran, B. Kellenberger, R. Flamary, D. Tuia, and N. Courty. Deepjdot: Deep joint distribution optimal transport for unsupervised domain adaptation. In *ECCV*, pages 467–483. Springer, 2018.
- [18] C. De Sa, A. Gu, C. Ré, and F. Sala. Representation tradeoffs for hyperbolic embeddings. *ICML*, 80:4460, 2018.
- [19] O. Demirel and E. Soytürk. The hyperbolic carnot theorem in the poincaré disc model of hyperbolic geometry. *Novi Sad J. Math.*, 38:33–39, 2008.
- [20] S. Ferradans, N. Papadakis, G. Peyré, and J.-F. Aujol. Regularized discrete optimal transport. *SIAM Journal on Imaging Sciences*, 7:1853–1882, 2014.
- [21] R. Flamary and N. Courty. Pot python optimal transport library. *GitHub*: <https://github.com/rflamary/POT>, 2017.
- [22] R. Flamary, K. Lounici, and A. Ferrari. Concentration bounds for linear monge mapping estimation and optimal transport domain adaptation. *arXiv preprint arXiv:1905.10155*, 2019.

- [23] M. Fréchet. Les éléments aléatoires de nature quelconque dans un espace distancié. In *Annales de l'institut Henri Poincaré*, volume 10, pages 215–310, 1948.
- [24] O. Ganea, G. Bécigneul, and T. Hofmann. Hyperbolic neural networks. In *NeurIPS*, pages 5345–5355, 2018.
- [25] O.-E. Ganea, G. Bécigneul, and T. Hofmann. Hyperbolic entailment cones for learning hierarchical embeddings. In *ICML*, 2018.
- [26] A. Genevay, G. Peyre, and M. Cuturi. Learning generative models with sinkhorn divergences. In *AISTATS*, pages 1608–1617, 2018.
- [27] X. Glorot and Y. Bengio. Understanding the difficulty of training deep feedforward neural networks. In *AISTATS*, pages 249–256, 2010.
- [28] C. Gulcehre, M. Denil, M. Malinowski, A. Razavi, R. Pascanu, K. M. Hermann, P. Battaglia, V. Bapst, D. Raposo, A. Santoro, et al. Hyperbolic attention networks. In *ICLR*, 2018.
- [29] V. Khruikov, L. Mirvakhabova, E. Ustinova, I. Oseledets, and V. Lempitsky. Hyperbolic image embeddings. In *CVPR*, pages 6418–6428, 2020.
- [30] S. Kim and J. Lawson. Unit balls, lorentz boosts, and hyperbolic geometry. *Results in Mathematics*, 63:1225–1242, 2013.
- [31] D. P. Kingma and J. Ba. Adam: A method for stochastic optimization. *ICLR*, 2015.
- [32] M. Knott and C. S. Smith. On the optimal mapping of distributions. *Journal of Optimization Theory and Applications*, 43:39–49, 1984.
- [33] M. Kochurov, S. Kozlukov, R. Karimov, and V. Yanush. Geoopt: Adaptive riemannian optimization in pytorch. <https://github.com/geoopt/geoopt>, 2019.
- [34] P. W. Lee and J. Li. New examples on spaces of negative sectional curvature satisfying Ma-Trudinger-Wang conditions. *SIAM Journal on Math. Anal.*, 44:61–73, 2012.
- [35] J. Li. *Smooth optimal transportation on hyperbolic space*. PhD thesis, Master’s thesis. University of Toronto, 2009.
- [36] Q. Liu, M. Nickel, and D. Kiela. Hyperbolic graph neural networks. In *NeurIPS*, pages 8228–8239, 2019.
- [37] X.-N. Ma, N. S. Trudinger, and X.-J. Wang. Regularity of potential functions of the optimal transportation problem. *Archive for rational mechanics and analysis*, 177:151–183, 2005.
- [38] A. Mallasto and A. Feragen. Wrapped gaussian process regression on riemannian manifolds. In *CVPR*, pages 5580–5588, 2018.
- [39] K. V. Mardia and P. E. Jupp. *Directional statistics*, volume 494. John Wiley & Sons, 2009.
- [40] V. Masarotto, V. M. Panaretos, and Y. Zemel. Procrustes metrics on covariance operators and optimal transportation of gaussian processes. *Sankhya A*, 81:172–213, 2019.
- [41] E. Mathieu, C. Le Lan, C. J. Maddison, R. Tomioka, and Y. W. Teh. Continuous hierarchical representations with poincaré variational auto-encoders. In *NeurIPS*, pages 12544–12555, 2019.
- [42] R. J. McCann. Polar factorization of maps on riemannian manifolds. *Geometric & Functional Analysis GFA*, 11:589–608, 2001.
- [43] R. J. McCann and N. Guillen. Five lectures on optimal transportation: geometry, regularity and applications. *Analysis and geometry of metric measure spaces: lecture notes of the séminaire de Mathématiques Supérieure (SMS) Montréal*, pages 145–180, 2011.

- [44] Y. Nagano, S. Yamaguchi, Y. Fujita, and M. Koyama. A wrapped normal distribution on hyperbolic space for gradient-based learning. In *ICML*, pages 4693–4702, 2019.
- [45] M. Nickel and D. Kiela. Poincaré embeddings for learning hierarchical representations. In *NeurIPS*, pages 6338–6347, 2017.
- [46] I. Ovinnikov. Poincaré wasserstein autoencoder. *arXiv preprint arXiv:1901.01427*, 2019.
- [47] A. Paszke, S. Gross, F. Massa, A. Lerer, J. Bradbury, G. Chanan, T. Killeen, Z. Lin, N. Gimelshein, L. Antiga, A. Desmaison, A. Kopf, E. Yang, Z. DeVito, M. Raison, A. Tejani, S. Chilamkurthy, B. Steiner, L. Fang, J. Bai, and S. Chintala. Pytorch: An imperative style, high-performance deep learning library. In *NeurIPS*, pages 8024–8035. Curran Associates, Inc., 2019.
- [48] O. Pele and M. Werman. Fast and robust earth mover’s distances. In *ICCV*, pages 460–467. IEEE, 2009.
- [49] X. Pennec. From riemannian geometry to computational anatomy. *Asclepios project-team, INRIA Sophia-Antipolis Mediterranee*, 71:72, 2011.
- [50] X. Pennec, S. Sommer, and T. Fletcher. *Riemannian Geometric Statistics in Medical Image Analysis*. Academic Press, 2020.
- [51] M. Perrot and A. Habrard. Regressive virtual metric learning. In *NeurIPS*, pages 1810–1818, 2015.
- [52] M. Perrot, N. Courty, R. Flamary, and A. Habrard. Mapping estimation for discrete optimal transport. In *NeurIPS*, pages 4197–4205, 2016.
- [53] G. Peyré, M. Cuturi, et al. Computational optimal transport. *Foundations and Trends® in Machine Learning*, 11:355–607, 2019.
- [54] A. Rakotomamonjy, R. Flamary, and N. Courty. Generalized conditional gradient: analysis of convergence and applications. *arXiv preprint arXiv:1510.06567*, 2015.
- [55] T. M. Rassias. *Mathematical Analysis and Applications*. Springer, 2000.
- [56] J. Ratcliffe. *Foundations of hyperbolic manifolds*, volume 149. Springer Science & Business Media, 2006.
- [57] R. Řehůřek and P. Sojka. Software Framework for Topic Modelling with Large Corpora. In *Proceedings of the LREC 2010 Workshop on New Challenges for NLP Frameworks*, pages 45–50, Valletta, Malta, May 2010. ELRA. <http://is.muni.cz/publication/884893/en>.
- [58] S. Said, L. Bombrun, and Y. Berthoumieu. Warped riemannian metrics for location-scale models. In *Geometric Structures of Information*, pages 251–296. Springer, 2019.
- [59] V. Seguy, B. B. Damodaran, R. Flamary, N. Courty, A. Rolet, and M. Blondel. Large-scale optimal transport and mapping estimation. In *ICLR*, pages 1–15, 2018.
- [60] S. Sommer, T. Fletcher, and X. Pennec. Introduction to differential and riemannian geometry. In *Riemannian Geometric Statistics in Medical Image Analysis*, pages 3–37. Elsevier, 2020.
- [61] Z. Sun, W. Hu, and C. Li. Cross-lingual entity alignment via joint attribute-preserving embedding. In *International Semantic Web Conference*, pages 628–644. Springer, 2017.
- [62] A. Tifrea, G. Bécigneul, and O.-E. Ganea. Poincaré glove: Hyperbolic word embeddings. In *ICLR*, 2019.

- [63] N. Trudinger and X.-J. Wang. On the second boundary value problem for monge-ampere type equations and optimal transportation. *Annali della Scuola Normale Superiore di Pisa-Classe di Scienze*, 8:143–174, 2009.
- [64] P. Tseng. Convergence of a block coordinate descent method for nondifferentiable minimization. *Journal of optimization theory and applications*, 109:475–494, 2001.
- [65] A. A. Ungar. *Analytic hyperbolic geometry and Albert Einstein's special theory of relativity*. World Scientific, 2008.
- [66] A. A. Ungar. A gyrovector space approach to hyperbolic geometry. *Synthesis Lectures on Mathematics and Statistics*, 1:1–194, 2008.
- [67] A. A. Ungar. *Analytic hyperbolic geometry in n dimensions: An introduction*. CRC Press, 2014.

.1 Data description

DBP15K [61]. It is a subtask from DBpedia, which is a large-scale multilingual knowledge base that includes inter-language links (ILLs) from entities of English version to those in other languages. The DBP15K dataset consists of 15 thousand ILLs with popular entities from English to Chinese, Japanese, and French respectively.

	DBP15K		Anatomy		Biodiv			
	English (EN)	French (FR)	Human	Mouse	FLOPO	PTO	ENVO	SWEET
Entities	19993	19661	3298	2737	360	1456	6461	4365
Relations	115722	105998	18556	7364	472	11283	73881	30101
Matched		14278		1517		154		402

Table 2: Dataset characteristics.

.2 Additional results

Domain adaptation on synthetic data. The aim of domain adaptation is to build a classifier such that said classifier trained on a domain (source) can be used to predict in a different domain (target). Fig. 4 shows an illustration of domain adaptation by aligning the hyperbolic embeddings of both domains.

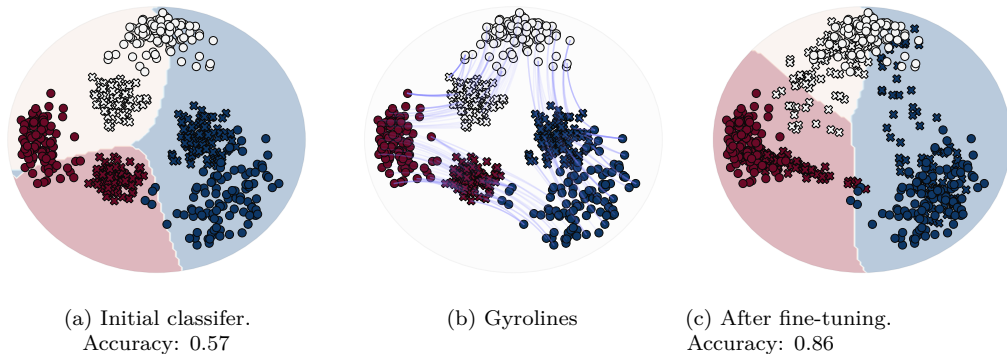


Figure 4: **Illustration on a toy example:** (a) Decision boundaries for shallow hyperbolic network trained on the source domain. (b) Gyrolines between samples matched according to the transport plan. (c) Decision boundaries after fine-tuning the classifier with samples transported to the target domain. Crosses depict the source domain, while class-colored circles are the target domain samples.

.3 Optimal transport on Riemannian manifolds

Brenier and McCann mappings. Brenier’s theorem states that the solution of the Monge problem can be characterized by the existence of the gradient of a convex function. McCann’s theorem [43, 42] generalizes the Brenier’s theorem to a general compact Riemannian manifold, (\mathcal{M}, ρ) . Let μ and ν be two probability measures compactly supported on \mathcal{M} , where μ is absolutely continuous with respect to the Riemannian volume. According to McCann, the optimal transport map T for the quadratic cost $c(\mathbf{x}, \mathbf{y}) = \frac{1}{2}d_s(\mathbf{x}, \mathbf{y})^2$ can be written as $T(\mathbf{x}) = \text{Exp}_{\mathbf{x}}(-\nabla\psi(\mathbf{x}))$, for some function ψ such that $\psi^{cc} = \psi$, where $u^c = \inf_{\mathbf{x} \in \mathcal{X}} \{c(\mathbf{x}, \mathbf{y}) - u(\mathbf{x})\}$ denotes the c -transform of u . A map u such that $u^{cc} = u$ is called c -concave.

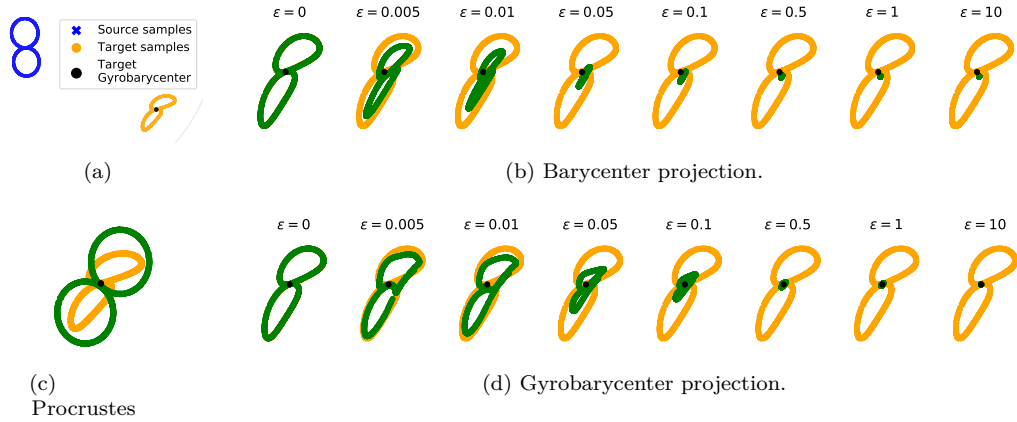


Figure 5: **Illustration of barycenter and gyrobaricenter mappings:** (a) Original samples; (b) Euclidean Barycenter mapping; (c) Orthogonal Procrustes with data centering; (d) Hyperbolic barycenter mapping (gyrobaricenter). The gyrobaricenter mapping collapses into gyromidpoint for a large enough entropic regularization parameter.

Some conditions for Regularity. Ma-Trudinger-Wang (MTW) conditions for regularity [37, 63] are sufficient for the optimal map to be smooth between a pair of log smooth bounded probability densities [43]. However, to use the squared-Riemannian distance of the hyperbolic space [35, 34] violates one of the MTW conditions as significant cut-locus issues arise in this context. Nevertheless, we can satisfy the MTW conditions for cost functions which are composition of a function l with a Riemannian distance of constant sectional curvature [34]. The Table 3 summarizes the MTW-regular cost functions.

cost function	MTW condition
$-\cosh \circ d$	strong
$-\log \circ (1 + \cosh) \circ d$	strong
$\pm \log \circ \cosh \circ d$	weak

Table 3: Hyperbolic cost functions that satisfy the strong/weak MTW conditions of regularity.

.4 Properties of Möbius operations

Equivalent hyperbolic distances.

$$\begin{aligned}
 d_s(\mathbf{x}, \mathbf{y}) &= 2s \tanh^{-1} \left(\frac{\|-\mathbf{x} \oplus_s \mathbf{y}\|}{s} \right) \\
 &= 2s \sinh^{-1} \left(\gamma_{\mathbf{x}} \gamma_{\mathbf{y}} \frac{\|\mathbf{x} - \mathbf{y}\|}{s} \right) \quad (\text{Theorem 7.4 [5]})
 \end{aligned} \tag{22}$$

We have $\lim_{s \rightarrow \infty} d_s(\mathbf{x}, \mathbf{y}) = 2d(\mathbf{x}, \mathbf{y})$ [65]. In particular, if we compute the distance to $\mathbf{0}$ [56, 30], it reduces to

$$\begin{aligned}
 d_s(\mathbf{0}, \mathbf{w}) &= 2s \tanh^{-1} \left(\frac{\|\mathbf{w}\|}{s} \right) \\
 &= 2s \sinh^{-1} \left(\gamma_{\mathbf{w}} \frac{\|\mathbf{w}\|}{s} \right).
 \end{aligned} \tag{23}$$

The Möbius scalar multiplication. It is defined as

$$r \otimes_s \mathbf{x} = s \tanh \left(r \tanh^{-1} \left(\frac{\|\mathbf{x}\|}{s} \right) \right) \frac{\mathbf{x}}{\|\mathbf{x}\|} \tag{24}$$

Group identity	Name/reference
$\ominus(\ominus a) = a$	involution of inversion
$\ominus a \oplus (a \oplus x) = x$	Left cancellation law
$\text{gyr}[a, b]c = \ominus(a \oplus b) \oplus (a \oplus (b \oplus c))$	Gyrator identity
$\ominus(a \oplus b) = \text{gyr}[a, b](\ominus b \oplus a)$	cf. $(ab)^{-1} = b^{-1}a^{-1}$ in a group
$(\ominus a \oplus b) \oplus \text{gyr}[\ominus a, b](\ominus b \oplus c) = \ominus a \oplus c$	cf. $(a^{-1}b)(b^{-1}c) = a^{-1}c$ in a group
$\text{gyr}[\ominus a, \ominus b] = \text{gyr}[a, b]$	Even property
$\text{gyr}[b, a] = \text{gyr}^{-1}[a, b]$	Inversive symmetry
$\phi(\text{gyr}[a, b]c) = \text{gyr}[\phi(a), \phi(b)]\phi(c)$	Gyration preserving under a gyrogroup homomorphism ϕ
$L_a \circ L_b = L_{a \oplus b} \text{gyr}[a, b]$	Composition law for left gyrotranslations

Table 4: Group identities of Gyrovector addition [55].

where $r \in \mathbb{R}$ and $\mathbf{x} \in \mathbb{B}_s^d \setminus \{\mathbf{0}\}$. $\lim_{s \rightarrow \infty} r \otimes_s \mathbf{x} = r \mathbf{x}$ [65].

The Möbius scalar multiplication has the following identities [66]:

$$\begin{aligned}
1 \otimes \mathbf{a} &= \mathbf{a} && \text{Identity scalar multiplication} \\
(r_1 + r_2) \otimes \mathbf{a} &= r_1 \otimes \mathbf{a} \oplus r_2 \otimes \mathbf{a} && \text{scalar distributive law} \\
(r_1 r_2) \otimes \mathbf{a} &= r_1 \otimes (r_2 \otimes \mathbf{a}) && \text{scalar associative law} \\
\frac{|r| \otimes \mathbf{a}}{\|r \otimes \mathbf{a}\|} &= \frac{\mathbf{a}}{\|\mathbf{a}\|} && \text{scaling property}
\end{aligned} \tag{25}$$

Möbius matrix multiplication.

$$\mathbf{Q}^{\otimes_s}(\mathbf{x}) := s \tanh \left(\frac{\|\mathbf{Q}\mathbf{x}\|}{\|\mathbf{x}\|} \tanh^{-1} \left(\frac{\|\mathbf{x}\|}{s} \right) \right) \frac{\mathbf{Q}\mathbf{x}}{\|\mathbf{Q}\mathbf{x}\|}, \tag{26}$$

Here, there are some properties of the Möbius matrix multiplication [24]: $\mathbf{Q}^{\otimes_s}(\mathbf{x}) = \mathbf{0}$ if $\mathbf{M}\mathbf{x} = \mathbf{0}$. $\mathbf{Q} \in \mathcal{M}_{m,n}(\mathbb{R})$ and $\mathbf{x} \in \mathbb{B}_s^d$. $\mathbf{Q}^{\otimes}(\mathbf{x}) = \mathbf{Q}^{\otimes_s} \mathbf{x}$, then $(\mathbf{Q}' \mathbf{Q}^{\otimes_s}) \mathbf{x} = \mathbf{Q}' \otimes_s (\mathbf{Q}^{\otimes_s} \mathbf{x})$. $(r \mathbf{Q}) \otimes_s \mathbf{x} = r \otimes (\mathbf{Q} \otimes_s \mathbf{x})$ for $r \in \mathbb{R}$. $\mathbf{Q} \otimes_s \mathbf{x} = \mathbf{Q}\mathbf{x}$ for $\mathbf{Q}^T \mathbf{Q} = \mathbf{I}$ (rotations are preserved). $\lim_{s \rightarrow \infty} \mathbf{Q} \otimes_s \mathbf{x} = \mathbf{Q}\mathbf{x}$.

Möbius addition. For any $\mathbf{x}, \mathbf{y} \in \mathbb{B}_s^d$, the Möbius addition (hyperbolic translation [56]) is defined as

$$\mathbf{x} \oplus_s \mathbf{y} := \frac{\left(1 + \frac{2}{s^2} \langle \mathbf{x}, \mathbf{y} \rangle + \frac{1}{s^2} \|\mathbf{y}\|^2\right) \mathbf{x} + \left(1 - \frac{1}{s} \|\mathbf{x}\|^2\right) \mathbf{y}}{1 + \frac{2}{s^2} \langle \mathbf{x}, \mathbf{y} \rangle + \frac{1}{s^4} \|\mathbf{x}\|^2 \|\mathbf{y}\|^2}. \tag{27}$$

Moreover, we have $(-\mathbf{x}) \oplus_s \mathbf{x} = \mathbf{x} \oplus_s (-\mathbf{x}) = \mathbf{0}$ and $(-\mathbf{x}) \oplus_s (\mathbf{x} \oplus_s \mathbf{x}) = \mathbf{y}$ (left cancellation law). However, this operation is usually not commutative, i.e., $(\mathbf{x} \oplus_s \mathbf{y}) \oplus_s (-\mathbf{y}) \neq \mathbf{y}$ [67]. $\lim_{s \rightarrow \infty} \mathbf{x} \oplus_s \mathbf{y} = \mathbf{x} + \mathbf{y}$.

The table 4 presents the group identities of the Möbius addition.

Gyrolines. Let $\mathbf{v} = (-\mathbf{x}) \oplus_s \mathbf{y}$ be a gyrovector with tail \mathbf{x} and head \mathbf{y} . Then, the hyperbolic line or Gyroline is defined as:

$$L(t) = \mathbf{x} \oplus_s [t \otimes_s ((-\mathbf{x}) \oplus_s \mathbf{y})], \quad -\infty < t < \infty. \tag{28}$$

For $t \in [0, 1]$, the Möbius gyrolines are identical to the geodesics of the Poincaré disc model of hyperbolic geometry connecting points $\mathbf{x}, \mathbf{y} \in \mathbb{B}_s^d$ [67]. $\lim_{s \rightarrow \infty} L(t) = \mathbf{x} + t(\mathbf{y} - \mathbf{x})$.

Exponential and Logarithmic map. We can also represent the exponential and logarithmic map using the Möbius addition [24]. For any point $\mathbf{x} \in \mathbb{B}_s^d$, the exponential map $\text{Exp}_{\mathbf{x}} : T_{\mathbf{x}}\mathbb{B}_s^d \rightarrow \mathbb{B}_s^d$ and the logarithm map $\text{Log}_{\mathbf{x}} : \mathbb{B}_s^d \rightarrow T_{\mathbf{x}}\mathbb{B}_s^d$ are given for $\mathbf{v} \neq \mathbf{0}$ and $\mathbf{y} \neq \mathbf{x}$ by:

$$\text{Exp}_{\mathbf{x}}^s(\mathbf{v}) = \mathbf{x} \oplus_s \left(s \tanh \left(\frac{\lambda_{\mathbf{x}}^s \|\mathbf{v}\|}{2s} \right) \frac{\mathbf{v}}{\|\mathbf{v}\|} \right), \quad \text{Log}_{\mathbf{x}}^s(\mathbf{y}) = \frac{2s}{\lambda_{\mathbf{x}}^s} \tanh^{-1} \left(\frac{\|-\mathbf{x} \oplus_s \mathbf{y}\|}{s} \right) \frac{-\mathbf{x} \oplus_s \mathbf{y}}{\|-\mathbf{x} \oplus_s \mathbf{y}\|} \quad (29)$$

.5 Proofs of main theorems

We first prove two useful lemmas.

Lemma 1. For x and $a \in R_+$, we have:

$$\sinh^{-1} \frac{x}{a} \leq \sqrt{x \frac{\pi}{2}} \quad (30)$$

Proof.

$$\begin{aligned} \sinh^{-1} \frac{x}{a} &= \int_0^x \frac{du}{\sqrt{a^2 + u^2}} \\ &\leq \sqrt{\int_0^x du \int_0^x \frac{du}{a^2 + u^2}} \quad (\text{Cauchy Schwarz}) \\ &= \sqrt{x \tan^{-1} \left(\frac{x}{a} \right)}, \\ &\leq \sqrt{x \frac{\pi}{2}}, \quad 0 \leq \tanh^{-1} x \leq \pi/2, \text{ and } x \geq 0 \end{aligned}$$

□

Lemma 2 (Distortion of Möbius matrix multiplication). Let $r \in \mathbb{R}$, $\mathbf{L} \in \mathbb{R}^{n \times d}$, and $\mathbf{w} \in \mathbb{B}_s^d / \{\mathbf{0}\}$, then we have

$$d(\mathbf{0}, \mathbf{L}^{\otimes} \mathbf{w}) = \frac{\|\mathbf{L}\mathbf{w}\|}{\|\mathbf{w}\|} d(\mathbf{0}, \mathbf{w}) \quad (31)$$

Proof. For completeness, we recall the scaling property of Möbius scalar multiplication on hyperbolic distances [30]. Let $r \in \mathbb{R}$ and $\phi_{s,\mathbf{u}} = s \tanh^{-1} \left(\frac{\|\mathbf{u}\|}{s} \right)$ be the rapidity of $\mathbf{u} \in \mathbb{B}_s^d$,

$$\begin{aligned} d_s(\mathbf{0}, r \otimes_s \mathbf{w}) &= 2s \tanh^{-1} \left(\frac{\|r \otimes_s \mathbf{w}\|}{s} \right) \\ &= 2s \tanh^{-1} \left(\frac{1}{s} \left\| s \tanh(r \phi_{s,\mathbf{w}}) \frac{\mathbf{w}}{\|\mathbf{w}\|} \right\| \right) \quad (\text{Definition of Möbius scalar mult.}) \\ &= 2s \tanh^{-1} (|\tanh(r \phi_{s,\mathbf{w}})|) \\ &= 2s \tanh^{-1} (\tanh(|r| \phi_{s,\mathbf{w}})) \quad (\text{Scaling prop. Eq. 25}) \\ &= 2s|r| \tanh^{-1} \left(\frac{\|\mathbf{w}\|}{s} \right) \\ &= |r| d_s(\mathbf{0}, \mathbf{w}) \end{aligned}$$

Rewriting the definition of Möbius matrix multiplication (Eq.24) in terms of the Möbius scalar multiplication,

$$\mathbf{M}^{\otimes_s}(\mathbf{x}) = \left(\frac{\|\mathbf{M}\mathbf{x}\|}{\|\mathbf{x}\|} \otimes_s \mathbf{x} \right) \frac{\|\mathbf{x}\|}{\mathbf{x}} \frac{\mathbf{M}\mathbf{x}}{\|\mathbf{M}\mathbf{x}\|} \quad (32)$$

Taking the norm of Eq. 32 and plugging it in Eq. 31 gives the desired result. □

Hyperbolic linear layer

We present the consistency of the Möbius matrix multiplication. We use uniform stability to show that our approach is consistent. An Euclidean version of this proof is presented in [51] and applied to OT-mapping estimation in [52].

We denote $\|\cdot\|_F$ the Frobenius norm of a matrix. Let $\mathbf{x}_i \in \mathcal{X}$, $\mathbf{y}_i \in \mathcal{Y}$ for $i \in [n]$, and $f : \mathcal{X} \rightarrow \mathcal{Y}$. We define the loss (Eq. 33), the empirical risk (Eq. 34), the empirical regularized risk (Eq. 36), the empirical risk on truncated training set (Eq. 35), and the empirical regularized risk on truncated training set (Eq. 37).

$$\ell(f, (\mathbf{x}, \mathbf{y})) = d_s(f(\mathbf{x}), \mathbf{y}), \quad (\text{Hyperbolic distance}) \quad (33)$$

$$\hat{R}(f) = \frac{1}{n} \sum_{j=1}^n \ell(f, (\mathbf{x}_j, \mathbf{y}_j)), \quad (34)$$

$$\hat{R}^{\setminus i}(f) = \frac{1}{n} \sum_{j \neq i}^n \ell(f, (\mathbf{x}_j, \mathbf{y}_j)), \quad (35)$$

$$\hat{R}_r(f) = \frac{1}{n} \sum_{j=1}^n \ell(f, (\mathbf{x}_j, \mathbf{y}_j)) + \omega \Omega(f), \quad (36)$$

$$\hat{R}_r^{\setminus i}(f) = \frac{1}{n} \sum_{j \neq i}^n \ell(f, (\mathbf{x}_j, \mathbf{y}_j)) + \omega \Omega(f), \quad (37)$$

where $\Omega(\cdot)$ is the regularization term, and $\omega \geq 0$ is the regularization parameter.

The quality loss of the hyperbolic mapping estimation is:

$$T \leftarrow \arg \min_{T \in \mathcal{T}} g(T) := \frac{1}{n} \sum_{i=1}^n \ell(T, (\mathbf{x}_i, \mathbf{y}_i)) + \omega \Omega(T), \quad (38)$$

where $\mathbf{y}_i = B_M^H(\mathbf{x}_i)$ for $i \in [n]$.

We use the set of hyperbolic linear transformations induced by a real matrix $\mathbf{L} \in \mathbb{R}^{d \times p}$ in this analysis:

$$\mathcal{T} = \left\{ T : \exists \mathbf{L} \in \mathbb{R}^{d \times p}, \forall \mathbf{x} \in \mathcal{X}, T(\mathbf{x}) = (\mathbf{L}^{\otimes s} \mathbf{x})^\top \right\}. \quad (39)$$

In our setting, let $\mathbf{x} \in \mathbb{B}_s^d$ and $\mathbf{v} \in \mathbb{B}_s^d$ be in the Poincaré ball of d dimensions and radius s . We assume $\|\mathbf{x}\| \leq C_x < s$ and $\|\mathbf{y}\| \leq C_y \leq s$. Then, using the definition of hyperbolic distances to zero Eq. 23, we have $d_s(\mathbf{0}, \mathbf{x}) \leq d_s(\mathbf{0}, C_x) = K_x$ and $d_s(\mathbf{0}, \mathbf{y}) \leq d_s(\mathbf{0}, C_y) = K_y$, as the $\tanh^{-1}(\cdot)$ is monotonically increasing.

Lemma 3. *Let \mathbf{L} be an optimal solution of Problem 38, we have:*

$$\|\mathbf{L}\|_F \leq \frac{K_y}{\omega} \quad (40)$$

Proof.

$$\begin{aligned} g(\mathbf{L}) &\leq g(\mathbf{0}) \\ \hat{R}(\mathbf{L}) + \omega \|\mathbf{L}\|_F &\leq \hat{R}(\mathbf{0}) + \omega \|\mathbf{0}\|_F \quad (\text{optimality of } \mathbf{L}) \\ \omega \|\mathbf{L}\|_F &\leq \frac{1}{n} \sum_{j=1}^n d_s(\mathbf{0}, \mathbf{v}_j) \quad (\text{problem 38 is always positive}) \\ \|\mathbf{L}\|_F &\leq \frac{K_y}{\omega} \quad (d_s(\mathbf{0}, \mathbf{v}) \leq K_y) \end{aligned}$$

□

Lemma 4. The loss $\ell(\mathbf{L}, (\mathbf{x}, \mathbf{v}))$ is bounded by $M = K_y \left(\frac{K_x}{\omega} + 1 \right)$

Proof.

$$\begin{aligned}
\ell(\mathbf{L}, (\mathbf{x}, \mathbf{v})) &= d_s(\mathbf{v}, \mathbf{L}^{\otimes} \mathbf{x}) \\
&\leq d_s(\mathbf{0}, \mathbf{L}^{\otimes} \mathbf{x}) + d_s(\mathbf{0}, \mathbf{v}) \quad (\text{Triangle ineq.}) \\
&= \frac{\|\mathbf{L}\mathbf{x}\|}{\|\mathbf{x}\|} d_s(\mathbf{0}, \mathbf{x}) + d_s(\mathbf{0}, \mathbf{v}) \quad (\text{Eq. 31}) \\
&\leq \|\mathbf{L}\|_F d_s(\mathbf{0}, \mathbf{x}) + d_s(\mathbf{0}, \mathbf{v}) \quad (\text{Prop. of norms}) \\
&\leq \|\mathbf{L}\|_F K_x + K_y \quad (d_s(\mathbf{0}, \mathbf{x}) \leq K_x, d_s(\mathbf{0}, \mathbf{v}) \leq K_y) \\
&\leq K_y \left(\frac{K_x}{\omega} + 1 \right) \quad (\text{Lemma 3})
\end{aligned}$$

□

Lemma 5. Upper bound of the Lorentz gamma factor of $\mathbf{P}^{\otimes} \mathbf{x}$ for $\mathbf{x} \in \mathbb{B}_s^d$ where $d_s(\mathbf{0}, \mathbf{x}) \leq K_x$:

$$\gamma_{\mathbf{P}^{\otimes} \mathbf{x}} \leq \exp \left(\frac{\|\mathbf{P}\|_F^2 K_x^2}{s^2} \frac{K_x^2}{8} \right). \quad (41)$$

Proof.

$$\begin{aligned}
\gamma_{\mathbf{P}^{\otimes} \mathbf{x}} &= \frac{1}{\sqrt{1 - \frac{\|\mathbf{P}^{\otimes} \mathbf{x}\|^2}{s^2}}} \leq \frac{1}{\sqrt{1 - \tanh^2 \left(\frac{\|\mathbf{P}\|_F K_x}{s} \right)}} \quad (\text{Eq. 43}) \\
&= \cosh \left(\frac{\|\mathbf{P}\|_F K_x}{s} \right) \\
&\leq \exp \left(\frac{\|\mathbf{P}\|_F^2 K_x^2}{s^2} \frac{K_x^2}{8} \right) \quad (\cosh x \leq \exp(x^2/2))
\end{aligned}$$

□

Lemma 6. Let $\|\mathbf{x}\| \leq C_x$, \mathbf{P} and \mathbf{Q} in $\mathbb{R}^{n \times n}$. If the matrices \mathbf{P} and \mathbf{Q} satisfy $\frac{1}{\|\mathbf{P}\mathbf{x}\|}, \frac{1}{\|\mathbf{Q}\mathbf{x}\|} \leq L$, then

$$\|\mathbf{P}^{\otimes} \mathbf{x} - \mathbf{Q}^{\otimes} \mathbf{x}\| \leq 2s L C_x \|\mathbf{P} - \mathbf{Q}\|_F. \quad (42)$$

Proof. Let us define

$$\begin{aligned}
k_1(\mathbf{x}) &= \left(\frac{\|\mathbf{P}\mathbf{x}\|}{\|\mathbf{x}\|} \otimes \|\mathbf{x}\| \right) \frac{1}{\|\mathbf{P}\mathbf{x}\|} \leq s \frac{1}{\|\mathbf{P}\mathbf{x}\|}, \\
k_2(\mathbf{x}) &= \left(\frac{\|\mathbf{Q}\mathbf{x}\|}{\|\mathbf{x}\|} \otimes \|\mathbf{x}\| \right) \frac{1}{\|\mathbf{Q}\mathbf{x}\|} \leq s \frac{1}{\|\mathbf{Q}\mathbf{x}\|}.
\end{aligned}$$

We assume w.l.o.g $k_2(\mathbf{x}) > k_1(\mathbf{x})$

$$\begin{aligned}
\|\mathbf{P}^{\otimes} \mathbf{x} - \mathbf{Q}^{\otimes} \mathbf{x}\| &= \|k_1(\mathbf{x})(\mathbf{P}\mathbf{x} - \mathbf{Q}\mathbf{x}) - (k_2(\mathbf{x}) - k_1(\mathbf{x}))\mathbf{Q}\mathbf{x}\| \quad (\text{Rewriting}) \\
&\leq k_1(\mathbf{x}) \|\mathbf{P}\mathbf{x} - \mathbf{Q}\mathbf{x}\| + (k_2(\mathbf{x}) - k_1(\mathbf{x})) \|\mathbf{Q}\mathbf{x}\| \quad (\text{Triangle ineq.}) \\
&\leq s \left\| \frac{1}{\|\mathbf{P}\mathbf{x}\|} \|\mathbf{P}\mathbf{x} - \mathbf{Q}\mathbf{x}\| + \left(\frac{1}{\|\mathbf{Q}\mathbf{x}\|} - \frac{1}{\|\mathbf{P}\mathbf{x}\|} \right) \|\mathbf{Q}\mathbf{x}\| \right\| \quad (\text{Subadditivity of } |\cdot|) \\
&\leq \frac{s}{\|\mathbf{P}\mathbf{x}\|} \|\mathbf{P}\mathbf{x} - \mathbf{Q}\mathbf{x}\| + \|\|\mathbf{P}\mathbf{x}\| - \|\mathbf{Q}\mathbf{x}\|\| \\
&\leq \frac{2s}{\|\mathbf{P}\mathbf{x}\|} \|\mathbf{P}\mathbf{x} - \mathbf{Q}\mathbf{x}\| \quad (\text{Reverse triangle ineq.}) \\
&\leq 2s L \|\mathbf{P}\mathbf{x} - \mathbf{Q}\mathbf{x}\| \quad \left(\frac{1}{\|\mathbf{P}\mathbf{x}\|} \leq L \right) \\
&\leq 2s L C_x \|\mathbf{P} - \mathbf{Q}\|_F \quad (\text{Prop. of norms and } \|\mathbf{x}\| \leq C_x)
\end{aligned}$$

□

Lemma 7 (Upper bound of the norm the Möbius matrix multiplication). *Let $\mathbf{x} \in \mathbb{B}_s^d$ with $\|\mathbf{x}\| \leq C_x$ and $d_s(\mathbf{0}, \mathbf{x}) \leq K_x$. Then,*

$$\|\mathbf{P}^{\otimes} \mathbf{x}\| \leq s \tanh\left(\frac{\|\mathbf{P}\|_F K_x}{s} \frac{K_x}{2}\right). \quad (43)$$

Proof.

$$\begin{aligned} \|\mathbf{P}^{\otimes} \mathbf{x}\| &= \frac{\|\mathbf{P}\mathbf{x}\|}{\|\mathbf{x}\|} \otimes \|\mathbf{x}\| && \text{(Rewritting)} \\ &= s \tanh\left(\frac{\|\mathbf{P}\mathbf{x}\|}{\|\mathbf{x}\|} \tanh^{-1}\left(\frac{\|\mathbf{x}\|}{s}\right)\right) \\ &\leq s \tanh\left(\|\mathbf{P}\mathbf{x}\| \frac{K_x}{2s\|\mathbf{x}\|}\right) && (d(\mathbf{0}, \mathbf{x}) \leq K_x) \\ &\leq s \tanh\left(\frac{\|\mathbf{P}\|_F K_x}{s} \frac{K_x}{2}\right). && \text{(Prop. of norms)} \end{aligned}$$

□

Lemma 8 (ℓ_∞ bound of the hyperbolic loss). *Let $\mathbf{x}, \mathbf{v} \in \mathbb{B}_s^d \setminus \{\mathbf{0}\}$ with $\|\mathbf{x}\| \leq C_x$, and \mathbf{P}, \mathbf{Q} in $\mathbb{R}^{n \times d}$, where \mathbf{P} and \mathbf{Q} satisfy $\frac{1}{\|\mathbf{P}\mathbf{x}\|}, \frac{1}{\|\mathbf{Q}\mathbf{x}\|} \leq L$, then*

$$|\ell(\mathbf{P}, (\mathbf{x}, \mathbf{v})) - \ell(\mathbf{Q}, (\mathbf{x}, \mathbf{v}))| \leq \sqrt{2\pi s^3 LC_x} (\|\mathbf{P} - \mathbf{Q}\|_F + 1) \quad (44)$$

Proof. Note that

$$|\ell(\mathbf{P}, (\mathbf{x}, \mathbf{v})) - \ell(\mathbf{Q}, (\mathbf{x}, \mathbf{v}))| \leq d(\mathbf{P}^{\otimes} \mathbf{x}, \mathbf{Q}^{\otimes} \mathbf{x}) \quad \text{(Reverse triangle ineq. [19])} \quad (45)$$

$$d(\mathbf{P}^{\otimes} \mathbf{x}, \mathbf{Q}^{\otimes} \mathbf{x}) = 2s \sinh^{-1}\left(\frac{\gamma_{\mathbf{P}^{\otimes} \mathbf{x}} \gamma_{\mathbf{Q}^{\otimes} \mathbf{x}} \|\mathbf{P}^{\otimes} \mathbf{x} - \mathbf{Q}^{\otimes} \mathbf{x}\|}{s}\right) \quad \text{(Eq. 22)}$$

$$\leq 2s \sinh^{-1}\left(\exp\left(\frac{\|\mathbf{P}\|_F^2 + \|\mathbf{Q}\|_F^2}{s^2} \frac{K_x^2}{8}\right) \frac{\|\mathbf{P}^{\otimes} \mathbf{x} - \mathbf{Q}^{\otimes} \mathbf{x}\|}{s}\right) \quad \text{(Eq. 41)}$$

$$\leq 2s \sqrt{\frac{\pi}{2}} \|\mathbf{P}^{\otimes} \mathbf{x} - \mathbf{Q}^{\otimes} \mathbf{x}\| \quad \text{(Eq. 30)}$$

$$\leq 2s \sqrt{2\pi s LC_x} \|\mathbf{P} - \mathbf{Q}\|_F \quad \text{(Eq. 42)}$$

$$\leq \sqrt{2\pi s^3 LC_x} (\|\mathbf{P} - \mathbf{Q}\|_F + 1) \quad (\sqrt{a} \leq (a+1)/2)$$

□

Lemma 9 (Majorizer of the hyperbolic distance of linear combination of matrices in Möbius matrix multiplication). *Let \mathbf{x} and \mathbf{v} in \mathbb{B}_s^d with $d_s(\mathbf{0}, \mathbf{v}) \leq K_y$. For $t \in [0, 1]$ we have:*

$$d(\mathbf{v}, [t\mathbf{P} + (1-t)\mathbf{Q}]^{\otimes s} \mathbf{x}) \leq t d(\mathbf{v}, \mathbf{P}^{\otimes s} \mathbf{x}) + (1-t) d(\mathbf{v}, \mathbf{Q}^{\otimes s} \mathbf{x}) + 2K_y \quad (46)$$

Proof.

$$d(\mathbf{v}, [t\mathbf{P} + (1-t)\mathbf{Q}]^{\otimes s} \mathbf{x})$$

$$\leq |d(\mathbf{0}, [t\mathbf{P} + (1-t)\mathbf{Q}]^{\otimes s} \mathbf{x}) + d(\mathbf{0}, \mathbf{v})|, \quad \text{(Triangle ineq.)}$$

$$= \left| \frac{\|[t\mathbf{P} + (1-t)\mathbf{Q}]^{\otimes s} \mathbf{x}\|}{\|\mathbf{x}\|} d(\mathbf{0}, \mathbf{x}) + d(\mathbf{0}, \mathbf{v}) \right|, \quad \text{(Eq. 31)}$$

$$\leq |t d(\mathbf{0}, \mathbf{P}^{\otimes s} \mathbf{x}) + (1-t) d(\mathbf{0}, \mathbf{Q}^{\otimes s} \mathbf{x}) + d(\mathbf{0}, \mathbf{v})| \quad \text{(Convexity of } \|\cdot\|)$$

$$\leq |t [d(\mathbf{0}, \mathbf{P}^{\otimes s} \mathbf{x}) - d(\mathbf{0}, \mathbf{v})] + (1-t) [d(\mathbf{0}, \mathbf{Q}^{\otimes s} \mathbf{x}) - d(\mathbf{0}, \mathbf{v})]| + |2d(\mathbf{0}, \mathbf{v})| \quad \text{(Subadditivity of } |\cdot|)$$

$$\leq |t d(\mathbf{v}, \mathbf{P}^{\otimes s} \mathbf{x}) + (1-t) d(\mathbf{v}, \mathbf{Q}^{\otimes s} \mathbf{x})| + |2d(\mathbf{0}, \mathbf{v})| \quad \text{(Reverse triangle ineq.)}$$

$$\leq t d(\mathbf{v}, \mathbf{Q}^{\otimes s} \mathbf{x}) + (1-t) d(\mathbf{v}, \mathbf{Q}^{\otimes s} \mathbf{x}) + 2K_y$$

□

Lemma 10. Let $T(\mathbf{x}) = \mathbf{L}^\otimes \mathbf{x}$. We denote \mathbf{L} a minimizer of \hat{R}_r and for $i \in [n]$, let \mathbf{L}^i denote a minimizer of $\hat{R}_r^{\setminus i}$. Then,

$$\|\mathbf{L}\|_F^2 - \|\mathbf{L}^i + t \Delta \mathbf{L}\|_F^2 + \|\mathbf{L}^i\|_F^2 - \|\mathbf{L}^i - t \Delta \mathbf{L}\|_F^2 \leq \frac{\sqrt{8\pi s^3 LC_x}}{\omega n} (t \|\Delta \mathbf{L}\|_F + 1) + \frac{4K_y}{\omega n} \quad (47)$$

Proof. Let \hat{R}_r and $\hat{R}_r^{\setminus i}$ be the functions to optimize, \mathbf{L} and \mathbf{L}^i their respective minimizers and ω the regularization parameter used in our algorithm. Let $\Delta \mathbf{L} = \mathbf{L} - \mathbf{L}^i$, then applying Lemma 9 for $t \in [0, 1]$:

$$\hat{R}_{\text{emp}}^{\setminus i}(\mathbf{L} - t \Delta \mathbf{L}) \leq t \hat{R}_{\text{emp}}^{\setminus i}(\mathbf{L}^i) + (1-t) \hat{R}_{\text{emp}}^{\setminus i}(\mathbf{L}) + \frac{2K_y}{n} \quad (48)$$

$$\hat{R}_{\text{emp}}^{\setminus i}(\mathbf{L}^i + t \Delta \mathbf{L}) \leq t \hat{R}_{\text{emp}}^{\setminus i}(\mathbf{L}) + (1-t) \hat{R}_{\text{emp}}^{\setminus i}(\mathbf{L}^i) + \frac{2K_y}{n} \quad (49)$$

Summing both inequalities,

$$\hat{R}_{\text{emp}}^{\setminus i}(\mathbf{L} - t \Delta \mathbf{L}) + \hat{R}_{\text{emp}}^{\setminus i}(\mathbf{L}^i + t \Delta \mathbf{L}) - \hat{R}_{\text{emp}}^{\setminus i}(\mathbf{L}) - \hat{R}_{\text{emp}}^{\setminus i}(\mathbf{L}^i) - \frac{4K_y}{n} \leq 0 \quad (50)$$

Let \mathbf{L} and \mathbf{L}^i be minimizer of Eq. 48 and Eq. 49, then

$$\begin{aligned} \hat{R}_r(\mathbf{L}) - \hat{R}_r(\mathbf{L} - t \Delta \mathbf{L}) &\leq 0, \\ \hat{R}_r^{\setminus i}(\mathbf{L}^i) - \hat{R}_r^{\setminus i}(\mathbf{L}^i + t \Delta \mathbf{L}) &\leq 0 \end{aligned} \quad (51)$$

Adding inequalities in Eq. 51 and Eq. 50,

$$\begin{aligned} \hat{R}_{\text{emp}}(\mathbf{L}) - \hat{R}_{\text{emp}}(\mathbf{L} - t \Delta \mathbf{L}) + \hat{R}_{\text{emp}}^{\setminus i}(\mathbf{L} - t \Delta \mathbf{L}) - \hat{R}_{\text{emp}}^{\setminus i}(\mathbf{L}) \\ \omega \|\mathbf{L}\|_F^2 - \omega \|\mathbf{L}^i + t \Delta \mathbf{L}\|_F^2 + \omega \|\mathbf{L}^i\|_F^2 - \omega \|\mathbf{L}^i - t \Delta \mathbf{L}\|_F^2 - \frac{4K_y}{n} \leq 0 \end{aligned}$$

Then,

$$\|\mathbf{L}\|_F^2 - \|\mathbf{L}^i + t \Delta \mathbf{L}\|_F^2 + \|\mathbf{L}^i\|_F^2 - \|\mathbf{L} - t \Delta \mathbf{L}\|_F^2 \leq \frac{B}{\omega} + \frac{4K_y}{\omega n}$$

$$\begin{aligned} B &\leq \left| \hat{R}_{\text{emp}}^{\setminus i}(\mathbf{L}) - \hat{R}_{\text{emp}}^{\setminus i}(\mathbf{L} - t \Delta \mathbf{L}) + \hat{R}_{\text{emp}}(\mathbf{L} - t \Delta \mathbf{L}) - \hat{R}_{\text{emp}}(\mathbf{L}) \right| \\ &= \left| \frac{1}{n} \sum_{(\mathbf{x}, \mathbf{v})^i \in S^i} \ell(\mathbf{L}, (\mathbf{x}, \mathbf{v})^i) - \frac{1}{n} \sum_{(\mathbf{x}, \mathbf{v})^i \in S^i} \ell(\mathbf{L} + t \Delta \mathbf{L}, (\mathbf{x}, \mathbf{v})^i) \right. \\ &\quad \left. + \frac{1}{n} \sum_{(\mathbf{x}, \mathbf{v}) \in S} \ell(\mathbf{L} + t \Delta \mathbf{L}, (\mathbf{x}, \mathbf{v})) - \frac{1}{n} \sum_{(\mathbf{x}, \mathbf{v}) \in S} \ell(\mathbf{L}, (\mathbf{x}, \mathbf{v})) \right| \\ &\leq \frac{1}{n} \left| \ell(\mathbf{L}, (\mathbf{x}_i, \mathbf{v}_i)) - \ell(\mathbf{L} + t \Delta \mathbf{L}, (\mathbf{x}_i, \mathbf{v}_i)) + \ell(\mathbf{L}, (\mathbf{x}_i, \mathbf{v}_i)^i) - \ell(\mathbf{L} + t \Delta \mathbf{L}, (\mathbf{x}_i, \mathbf{v}_i)^i) \right| \\ &\leq \frac{1}{n} \left| \ell(\mathbf{L}, (\mathbf{x}_i, \mathbf{v}_i)) - \ell(\mathbf{L} + t \Delta \mathbf{L}, (\mathbf{x}_i, \mathbf{v}_i)) \right| + \frac{1}{n} \left| \ell(\mathbf{L}, (\mathbf{x}_i, \mathbf{v}_i)^i) - \ell(\mathbf{L} + t \Delta \mathbf{L}, (\mathbf{x}_i, \mathbf{v}_i)^i) \right| \\ &\leq \frac{\sqrt{8\pi s^3 LC_x}}{n} (t \|\Delta \mathbf{L}\|_F + 1) \end{aligned}$$

□

where the second inequality comes from the fact that the sums differ by the i th-element. The last inequality uses lemma 8.

Definition 2 (Uniform stability [8]). An algorithm A has uniform stability β with respect to the loss function ℓ if the following holds

$$\forall S \in D, \forall i \in [n], \|\ell(A_S, \cdot) - \ell(A_{S \setminus \{i\}}, \cdot)\|_\infty \leq \beta.$$

Lemma 11. *Our algorithm has uniform stability $\beta = \frac{1}{2\omega n} \left(\frac{N_x^2}{4\omega n} + 2N_x + 8K_y + 1 \right)$, where $N_x = \sqrt{2\pi s^3 LC_x}$.*

Proof. Set $t = \frac{1}{2}$ on the left hand side of lemma 10,

$$\|\mathbf{L}\|_F^2 - \|\mathbf{L}^i + \frac{1}{2}\Delta\mathbf{L}\|_F^2 + \|\mathbf{L}^i\|_F^2 - \|\mathbf{L} - \frac{1}{2}\Delta\mathbf{L}\|_F^2 = \frac{1}{2}\|\Delta\mathbf{L}\|_F^2$$

and thus:

$$\begin{aligned} \frac{1}{2}\|\Delta\mathbf{L}\|_F^2 &\leq \frac{\sqrt{2\pi s^3 LC_x}}{\omega n} (\|\Delta\mathbf{L}\|_F + 1) + \frac{4K_y}{\omega n} \\ \|\Delta\mathbf{L}\|_F &\leq \frac{N_x}{2\omega n} + \frac{1}{\omega n} \sqrt{\frac{N_x^2}{4\omega n} + N_x + 8K_y}, \quad \text{where } N_x = \sqrt{2\pi s^3 LC_x}. \\ &\leq \frac{1}{2\omega n} \left(\frac{N_x^2}{4\omega n} + 2N_x + 8K_y + 1 \right) \quad (\sqrt{a} \leq (a+1)/2) \end{aligned}$$

□

Theorem 1 ([8]). *Let A be an algorithm with uniform stability β with respect to a loss function l such that $0 \leq l(A_S, z) \leq M$, for all $z \in \mathcal{Z}$ and all sets S . Then, for any $n \geq 1$, and any $\delta \in (0, 1)$, the following bounds hold (separately) with probability $1 - \delta$ over the random draw of the sample S*

$$R \leq \hat{R}_{emp} + 2\beta + (4n\beta + M) \sqrt{\frac{\ln 1/\delta}{2n}},$$

Theorem 2. *Let $\|\mathbf{y}\| \leq C_y$ and $\|\mathbf{x}\| \leq C_x$, for any \mathbf{x} and \mathbf{y} in $\mathbb{B}_s^d \setminus \{\mathbf{0}\}$ with a probability of $1 - \delta$ for any matrix \mathbf{L} optimal solution of problem 38 such that $\|\mathbf{L}\mathbf{x}\|^{-1} \leq L$ and $\|\mathbf{L}\mathbf{y}\|^{-1} \leq L$, we have:*

$$\begin{aligned} R(\mathbf{L}) &\leq \hat{R}_{emp}(\mathbf{L}) + \frac{1}{\omega n} \left(\frac{N_x^2}{4\omega n} + 2N_x + 8K_y + 1 \right) \\ &\quad + \left(\frac{2}{\omega} \left(\frac{N_x^2}{4\omega n} + 2N_x + 1 \right) + K_y \left(\frac{K_x + 16}{\omega} + 1 \right) \right) \sqrt{\frac{\ln(1/\delta)}{2n}}, \end{aligned} \tag{52}$$

where $N_x = 2s\sqrt{2\pi s LC_x}$.

Proof. As our algorithm is uniformly stable and our loss is bounded, hence we can apply Theorem 1, with $M = K_y \left(\frac{K_x}{\omega} + 1 \right)$ (lemma 4), and $\beta = \frac{1}{2\omega n} \left(\frac{N_x^2}{4\omega n} + 2N_x + 8K_y + 1 \right)$, where $N_x = \sqrt{2\pi s^3 LC_x}$ (lemma 11). □

Hyperbolic linear layer for mapping estimation

Theorem 3. *Let f^* be the true transport map. Let $B_{\mathbf{M}_0}(\mathbf{x})$ be the true barycentric mapping associated with the probabilistic coupling \mathbf{M}_0 . Let $B_{\hat{\mathbf{M}}}(\mathbf{x})$ be the empirical barycentric mapping of \mathbf{X}^s using the probabilistic coupling $\hat{\mathbf{M}}$ learned between \mathbf{X}^s and \mathbf{X}^t .*

$$\begin{aligned} \mathbb{E}_{\mathbf{x}^s \sim \mathcal{X}^s} [d(f(\mathbf{x}^s), f^*(\mathbf{x}^s))] &\leq \sum_{\mathbf{x}^s \in \mathcal{X}^s} d(f(\mathbf{x}^s), B_{\hat{\mathbf{M}}}(\mathbf{x}^s)) + \sum_{\mathbf{x}^s \in \mathcal{X}^s} d(B_{\hat{\mathbf{M}}}(\mathbf{x}^s), B_{\mathbf{M}_0}(\mathbf{x}^s)) \\ &\quad + O\left(\frac{1}{\sqrt{n^s}}\right) + \mathbb{E}_{\mathbf{x}^s \sim \mathcal{X}^s} [d(f^*(\mathbf{x}^s), B_{\mathbf{M}_0}(\mathbf{x}^s))] \end{aligned} \tag{53}$$

Proof.

$$\begin{aligned}
& \mathbb{E}_{\mathbf{x}^s \sim \mathcal{X}^s} [d(f(\mathbf{x}^s), f^*(\mathbf{x}^s))] \\
& \leq \mathbb{E}_{\mathbf{x}^s \sim \mathcal{X}^s} [d(f(\mathbf{x}^s), B_{\mathbf{M}_0}(\mathbf{x}^s))] + \mathbb{E}_{\mathbf{x}^s \sim \mathcal{X}^s} [d(f^*(\mathbf{x}^s), B_{\mathbf{M}_0}(\mathbf{x}))] \quad (\text{Triangle ineq.}) \\
& \leq \sum_{\mathbf{x}^s \in \mathcal{X}^s} d(f(\mathbf{x}^s), B_{\mathbf{M}_0}(\mathbf{x}^s)) + O\left(\frac{1}{\sqrt{n^s}}\right) + \mathbb{E}_{\mathbf{x}^s \sim \mathcal{X}^s} [d(f^*(\mathbf{x}^s), B_{\mathbf{M}_0}(\mathbf{x}^s))] \quad (\text{Eq. 52}) \\
& \leq \sum_{\mathbf{x}^s \in \mathcal{X}^s} d(f(\mathbf{x}^s), B_{\tilde{\mathbf{M}}}(\mathbf{x}^s)) + \sum_{\mathbf{x}^s \in \mathcal{X}^s} d(B_{\tilde{\mathbf{M}}}(\mathbf{x}^s), B_{\mathbf{M}_0}(\mathbf{x}^s)) + O\left(\frac{1}{\sqrt{n^s}}\right) \\
& \quad + \mathbb{E}_{\mathbf{x}^s \sim \mathcal{X}^s} [d(T^*(\mathbf{x}^s), B_{\mathbf{M}_0}(\mathbf{x}^s))] \quad (\text{Triangle ineq.})
\end{aligned}$$

□

Link with Wrapped Gaussian Distributions.

Definition 3. Let ν be a measure on X and $f : X \rightarrow Y$ be a measurable map. We define the push-forward as $f^\# \nu(A) := \nu(f^{-1}1(A))$ for any measurable set A in Y [38].

Definition 4 (Wrapped Gaussian [44, 39, 58]). Define $\mathbf{x} \sim (\text{Exp}_\mu)_\# \mathcal{N}(0, \Sigma)$ to be a wrapped Gaussian random variable with bias $\mu \in \mathbb{B}_s^d$ and covariance matrix $\Sigma \in \mathbb{R}^{n \times n}$. To build a wrapped Gaussian, we draw samples at random from a zero-mean Gaussian distribution with covariance Σ , $\mathbf{z} \sim \mathcal{N}(0, \Sigma)$. We project these samples onto the manifold at zero, $\bar{\mathbf{x}}_i = \text{Exp}_0(\mathbf{z}_i)$. Finally, we add the bias term μ using the Möbius addition, $\mathbf{x}_i = \text{Exp}_\mu(\mathbf{z}_i)$.

Theorem 4 (Optimal transport: Wrapped linear case). Let $\mathbf{x} \sim (\text{Exp}_{\mu_1}^s)_\# \mathcal{N}(0, \Sigma_1)$ and $\mathbf{y} \sim (\text{Exp}_{\mu_2}^s)_\# \mathcal{N}(0, \Sigma_2)$ be two hyperbolic random variables, distributed under wrapped Gaussian with parameters $\mu_i \in \mathbb{B}_s^d$ for $i = 1, 2$ and $\Sigma_i \in \mathbb{R}^{n \times n}$ for $i = 1, 2$. Then,

$$\begin{bmatrix} \mathbf{x} \\ \mathbf{y} \end{bmatrix} = \begin{bmatrix} \mathbf{x} \\ \mu_2 \oplus_s \mathbf{T}^\otimes (-\mu_1 \oplus_s \mathbf{x}) \end{bmatrix} \sim (\text{Exp}_{[\mu_1, \mu_2]}^s)_\# \mathcal{N}\left(\mathbf{0}, \begin{bmatrix} \Sigma_1 & \mathbf{T} \Sigma_1 \\ \Sigma_1 \mathbf{T} & \Sigma_2 \end{bmatrix}\right), \quad (54)$$

where $\mathbf{T} \in \text{Sym}^+(n)$ is the solution of the Riccati equation $\mathbf{T} \Sigma_1 \mathbf{T} = \Sigma_2$ [7, 22].

Proof. By the definition 4, let $\mathbf{x} = \mu_1 \oplus_c \bar{\mathbf{x}}$ and $\mathbf{y} = \mu_2 \oplus_c \bar{\mathbf{y}}$ be Gyrovectors in \mathbb{B}_s^d , where $\bar{\mathbf{x}}$ and $\bar{\mathbf{y}}$ are zero-mean wrapped-Gaussian vectors, $\bar{\mathbf{x}} \sim (\text{Exp}_0^s)_\# \mathcal{N}(\mathbf{0}, \Sigma_1)$ and $\bar{\mathbf{y}} \sim (\text{Exp}_0^s)_\# \mathcal{N}(\mathbf{0}, \Sigma_2)$ respectively. Thus, $\bar{\mathbf{x}} = (-\mu_1) \oplus_c \mathbf{x}$ by the left-cancellation law. Then, we solve the transport problem in the tangent space at $\mathbf{0}$, $T_0 \mathbb{B}_s^d$ for $\mathbf{u} = \text{Log}_0^s(\bar{\mathbf{x}})$ and $\mathbf{v} = \text{Log}_0^s(\bar{\mathbf{y}})$, which produces $\mathbf{v} = \mathbf{T} \mathbf{u}$. Finally, we use the exponential map at zero on both sides and add the bias term μ_2 on the left, obtaining $\mathbf{y} = \mu_2 \oplus_c \mathbf{T}^\otimes (-\mu_1 \oplus_s \mathbf{x})$. □

Relationship between the Gyrobarycenter and the Barycenter. As we stated it in the main manuscript, we defined the matrix form of the gyrobarycenter as:

$$B_{\mathbf{M}}^{\text{H}}(\mathbf{X}^s) = \frac{1}{2} \otimes_s \text{diag}(\mathbf{M} \mathbf{g})^{-1} \mathbf{M} \mathbf{G} \mathbf{X}^t, \quad (55)$$

where $\mathbf{g} = (\gamma_{\mathbf{X}}^s)^2 - \frac{1}{2}$, $\mathbf{G} = \text{diag}((\gamma_{\mathbf{X}}^s)^2)$, and $\gamma_{\mathbf{X}}^s$ denotes the Lorentz gamma factor applied sample-wise. We know that $\lim_{s \rightarrow \infty} \gamma_{\mathbf{X}}^s = 2$, then $\lim_{s \rightarrow \infty} \mathbf{G} = 4 \mathbf{I}$, where \mathbf{I} is the identity matrix. Similarly, $\lim_{s \rightarrow \infty} \mathbf{g} = \frac{7}{2} \mathbf{1}$. Finally, we know that $\lim_{s \rightarrow \infty} r \otimes_s \mathbf{x} = r \mathbf{x}$ (see Section .4). Hence,

$$\lim_{s \rightarrow \infty} B_{\mathbf{M}}^{\text{H}}(\mathbf{X}^s) = \frac{4}{7} B_{\mathbf{M}}^{\text{E}}(\mathbf{X}^s) \quad (56)$$